Visibility evaluation for intraocular lens with glistening by microscopic image analysis based on light scattering model

Kay Thwe Min Han

Japan Advanced Institute of Science and Technology

Doctoral Dissertation

Visibility evaluation for intraocular lens with glistening by microscopic image analysis based on light scattering model

Kay Thwe Min Han

Supervisor: Professor Kazunori Kotani

Graduate School of Advanced Science and Technology
Japan Advanced Institute of Science and Technology
Information Science

September 2020

Abstract

Visual function is decreased due to glistening and subsurface nanoglistening (whitening) after intraocular lens (IOL) implantation into human eyes. Glistening means fluid filled micro-sized vacuoles, on the other hand, whitening is nano-sized vacuoles in IOL which lead to light scattering and affect human's vision quality. Glistening observation and light scattering in IOL mainly depend on the characteristics of glistenings which are size, shape, refractive index, and number of glistenings. Furthermore, glistening occurrence in IOL depends on various conditions. Moreover, vision quality can also be different based on these facts. Glistening is increasingly over time and so it cannot be stopped by medicine and treatment. The best treatment for glistening is surgical removal and thus, the effect of glistening in IOL is required to study. We approach the light scattering problem from time and cost-effective way which evaluate the visibility of IOL.

Several researches studied glistenings from ophthalmology and assessed the consequence of glistening in vision quality by clinical tests such as contrast sensitivity, visual acuity and glare testing or wavefront measurements of the human eyes. This kind of research is required to participate by the patients and assessed light scattering in IOL by using clinical equipment such as C-Quant, spectrometer and Scheimpflug photography and thus, it is time consuming and costly to study. Moreover, these studies report the light scattering from single sphere particle but multiple particles scattering for IOL are not considered. For the real light scattering problem in IOL, light transmittance to the retina which can interfere by glistenings is not only for single particle, but also multi-glistenings. In multiple glistenings, the distance between particles are important in light scattering measurement of IOL. If the particles are brought closer together, so that their surfaces are from one another, then their scattering volumes begin to overlap. Therefore, the total scattering volume from the two glistenings is less than the sum of the two-individual scattering volumes. When light that enters the overlap volume, light can scatter less efficiently than light that enters a part of the non-overlapping scattering. Finally, there is no report to evaluate the visibility of IOL with glistenings to solve each of the above problems.

This research proposes optical model to study the glistenings in IOL with visibility evaluation from multiple light scattering with T-matrix method. However, this optical model considers the important facts to overcome the real problems which are not yet developed by the previous studies. When glistening numbers are grown, light scatter problem may occur inside the lens and vision quality will be degraded. Firstly, visibility function is evaluated based on the glistening characteristics in the optical model. When microvacuoles are densely located in IOL, light scattering for single particle is not sufficient and multiple light scattering is important to be considered. Therefore, multiple light scattering of glistenings are calculated by using T-matrix theory. Moreover, light transmission through Intraocular lens (IOL) with glistenings and whitenings are also computed. In fact, the proposed model study the characteristics of laboratory-induced glistenings under temperature changes, calculate the light scattering from multiple light scattering theory and simulate the light transmission to the retina.

Although light scattering is measured from different approaches, there is no research of light scattering effects differs depending upon the human activities. In this research, the most important approach is visibility evaluation in considered from human activities such as driving at night, studying and walking. Furthermore, this optical model evaluates visibility functions of IOL with glistenings through glare and quality of retinal image contrast. Glistenings give arise light scattering in IOL and as a result of intraocular light scatter called straylight in retina, disability glare. The quality of human vision depends on the image on the retina. Disability glare can cause the loss of retinal image contrast due to glistenings in IOL. Therefore, reduction of contrast due to glistenings are evaluated for visual functions and assessed the quality of the lens degradation. As a summary, this research combines all the important facts to model the visibility evaluation of intraocular lens with glistenings by microscopic image analysis based on light scattering model.

Key Words: **Visibility Evaluation, Optical Model, Multiple Light Scattering, T-matrix, Glistening**

Acknowledgments

I would like to express the deepest appreciation to my advisers Professor Kazunori Kotani, Associate Professor Waree Kongprawechnon, Assistant Professor Prarinya Siritanawan, and former advisor from SIIT, Dr. Bunyarit Uyyanonva for the patient guidance, encouragement, and advice they have provided throughout my time as their student. Without their guidance and persistent help, this dissertation would not have been possible. I would like to thank my committee members from JAIST, Professor KANEKO Mineo, Associate Professor HASEGAWA Shinobu, and Associate Professor IKEDA Kokolo for offering their time, comments, support, and guidance on this dissertation. Moreover, I am also thankful to committee members from SIIT and NECTEC(Thailand), Professor Stanislav S. Makhanov, Associate Professor Pakinee Aimmanee, and Dr.Chanjira Sinthanayothin for their thoughtful comments, recommendations, and intellectual contributions to this dissertation. I thank Japan Advanced Institute of Science and Technology for permission to submit the conference and journals. Furthermore, I would like to express my appreciation to Dr.Nattapon Wongcumchang, Dr.April Cho Aung, Dr.Zwe Zaw Zaw Naing, Dr.Aye Min Thant, and Dr. LaWun Phyu Phyu, medical doctors for providing me Intraocular lens(IOL) and knowledge of glistening formation in IOL. I also would like to extend my appreciation to Gunter, P'Chat, and Bell for the knowledge of microscope and microscopic images.

I would like to thank, SIIT-JAIST dual degree program, Sirindhorn International Institute of Technology (SIIT), Japan Advanced Institute of Science and Technology (JAIST), and National Electronics and Computer Technology Center (NECTEC) for providing me this opportunity and supporting me financially. I am thankful to my Myanmar, Thai, Japanese, and other international friends from SIIT and JAIST who assisted me in identifying relevant on living abroad and guided me throughout my work including coding, presenting, and report writing. Finally, my deep and sincere gratitude to my family for their continuous and unparalleled love, help, and support. I am forever indebted to my parents for giving me these opportunities and experiences that have made me who I am. Last but not least, I am forever thankful to my best friend, Mya Thandar for giving me a lot of encouragement, support, and continuous optimism to complete this dissertation. This journey would not have been possible if not for them, and I dedicate this milestone to them.

Contents

This dissertation was prepared according to the curriculum for the Collaborative Education Program organized by Japan Advanced Institute of Science and Technology and Thammasat University.

List of Figures

List of Tables

Chapter 1

Introduction

1.1 Overview of Visibility evaluation for intraocular lens with glistening based on light scattering model

Intraocular lens (IOL) is a lens which is implanted in human eyes to replace natural cloudy lens during cataract surgery. Degraded vision quality is related to the formation of glistening in IOL. Glistening is defined as microvacuoles inside the IOL optic when light passes through it. In fact, glistenings can be seen in all IOL materials but are mostly found with hydrophobic acrylic IOLs[1][2][3]. From the previous clinical study, glistening was found in 57% of IOL from 2 to 16 months after IOL implantation[4]. When IOL is implanted into human eyes, the temperature differences between the human body and the manufacturing process occur water gap inside the lens. There are many research studied glistenings from ophthalmology and assessed the consequence of glistening in vision quality by clinical tests such as contrast sensitivity, visual acuity, and glare testing or wavefront measurements of the human eyes. These studies required to participate by the patients and calculated light scattering manually and furthermore, it is time-consuming and costly to research. However, this research approach optical modeling in which visibility function is evaluated from glistening characteristics, human activities, and light scatter condition IOL. For this purpose, the input is IOL images with glistenings from human eyes, analyze these glistenings in IOL by image analysis, and develop an optical model to cope visibility evaluation of IOL. Figure 1.1 shows the fundamental steps of this research.

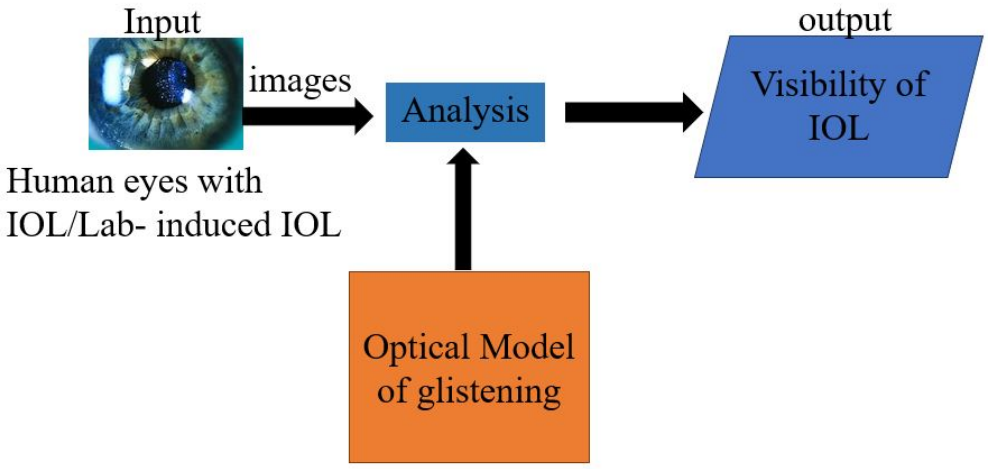

Figure 1.1: Basic concept of research

When light traverses into the human eye, it is refracted by cornea and lens to produce an image on the retina. In human eyes, the retina is the light-sensitive part of the eye in which fovea is located at a central region for high acuity of vision. Moreover, the cell structure of the retina is composed of rod and cone cells to be light-sensitive and the function of rod and cone cells are applied based on human activities such as driving at night time or studying at day time. However, rod cells are more light-sensitive than cone cells because these cells can be sensitive for the entire visible spectrum. Therefore, the wavelength of the light which passes through the lens to the retina is considered to be in the range of the human visible spectrum of rod and cones.

In general, glistenings can increase the intraocular stray light[5]. However, the stray light which impacts vision quality on the retina is associated with forward light scatter. Forward scattering means that light scattered towards the retina (angle between 0^{o} and 180^{o}), and can cause veiling illuminance on the retinal image which affects the reduction in contrast. In addition, light scattering may produce halos or glare due to the increasing of diffused light on the retina. However, the amount of intraocular stray light that can affect the vision quality depends on the characteristics of glistenings such as size, shape, refractive index, and the number of the glistening. According to previous studies, glistenings has been reported with the diameter range from 10 to 20 µm by Dogru et al. (2000) [6]. In addition, the different size of glistenings have been found by DeHoog et al. (2014) from 2 to 200 µm [7]. Henriksen et al (2015) separate the size of glistenings into two groups: 6 to 25 µm or greater than 25 µm [8]. Recently, the size of glistening is significantly varied and observed by Takahashi et al. (2015) with three different sizes: 100 nm, 150 nm, and 200 nm[9].

Next, the number of glistening in IOL is also an important factor for grading of glistening. Traditionally, glistenings are graded in the intraocular lens by clinicians through the slit lamp. They manually counted the number of glistenings and report as different grades. Therefore, several studies described grading by the number of glistenings present in IOL. Firstly, three grades of glistenings such as 1 +,2 +, and 3 + have been reported by Dhaliwal et al. (1996) [10]. Moreover, glistening grades are recorded as 0 to 3+ by Wilkins and Olson (2001)[11]. They denote 0 for no glistenings, 1+ for less than 10, 2+ for 10 to 50, and 3+ for more than 50. Yet, Cisneros-Lanuza et al.(2016) proposed

to grade 1+ for 10 to 20, 2+ for 20 to 30, 3+ for 30 to 40 and 4+ for more than 40 glistenings[12] .Glistening number are classified and measured per mm2 by Weindler et al. (2019) where grade 0 (none), grade 1 (1-100), grade 2 (101-200), grade 3 (201-500) and grade 4 (more than 500) [13]. According to previous studies, grading scales can be represented by the occurrence of glistening numbers in IOL, but a common agreement is not found on defining glistening's grading.

Glistenings can be seen in IOL because of the different refractive indices between the IOL material and water inside the IOL material. However, refractive index values are varied due to the material and type of IOL. For example, PMMA (1.49), silicone (1.43-1.46), hydrophilic acrylic (1.47), hydrophobic acrylic (1.47 to 1.55). Impact of light scattering caused from glistenings' IOL has been studied in [8][14][7][12]. The previous research [8][14][15] evaluated light scattering in IOL by using medical equipment such as straylight meter (C Quant log) and Scheimpflug photography. Nevertheless, other research analyzed from mathematically modeling with Mie scattering theory [7][16]. If particle shapes are sphere, Mie theory is more appropriate to solve the light scattering problem. Since the different shapes of glistenings have been found in IOL, multiple light scattering occurs. The single light scattering problem by a sphere is not sufficient to satisfy the problem.

Several studies report the light scattering from one sphere. Multiple scattering for IOL has not considered. In this research, T-Matrix method is applied for light scattering in IOL images by mathematical modeling and optical simulation to evaluate the visibility of IOL. In fact, T-matrix method calculated a pair of spherical particles as a single scatterer and has originally been developed by Waterman[17]. The proposed methodology aims to simulate multiple scattering in IOL, although many research used Mie scattering theory to model a single glistening. As a result, multiple light scattering of the electric field through glistenings in IOL can be calculated and simulated. Moreover, visual functions is evaluated from different light conditions and human activities. In this research, all of these important facts are combined as an optical model of IOL with glistenings and evaluate the visibility of human eyes with IOL.

1.2 Research Problem and Motivations

The visual functions that are complained after implantation is small bright particle formations called glistenings in IOL which is associated with light scattering. Since glistenings are possibly in any material and design of IOL, light scattering can be encountered by the patients after the following years of the IOL implantation [1][4][14]. When the incident light passes through a medium called an intraocular lens, light can be transmitted, reflected, and scattered to random directions due to glistenings. However, the previous studies[18] show that the direction of light scattering which is caused by glistening propagates backward and forward. Forward scattering increase the intraocular straylight and backward scattering decrease in light transmittance to the retina. Therefore, image quality which is received by the retina is correlated to light scattering in IOL and transmission to retina. Moreover, a light scattering of IOLs is associated with unwanted glare, optical defects, unclear image quality, and other phenomena that can affect daily activities. Hence, visibility evaluation is required from IOL with glistenings in which light scattering occurred inside the lens.

To assess light scattering in IOL, clinical studies used different types of equipment such as C-Quant, spectrometer, and Scheimpflug photography. This kind of research is costly and clinicians are also required to collaborate. Moreover, these research have the following drawbacks.

- Scheimpflug device did not provide images of required resolution to perform automated counting of separate glistenings[19].
- Glistenings less than 2µm in diameter cannot be detected smaller sizes with slit-lamp photographs[8].
- C-Quant instrument delivers the straylight parameter of the eye for a fixed visual angle. This might appear as a limitation as one may wonder about the straylight value at smaller or larger angular distances of the glare source[20].
- Glistening particles are aggregated based on the grade and shapes are also different. Light scattering in glistenings are calculated based on single particle scattering theory and near-field scattering effects are not considered.

Therefore, we approach the light scattering problem from time and cost-effective way which evaluates the visibility of IOL. Several research studied the quality of vision from a clinical assessment such as contrast sensitivity and visual acuity but the lifetime of the lens from affected glistenings is not reported. Moreover, these studies report the light scattering from a single sphere particle and multiple particle scattering for IOL are not considered. For the real light scattering problem in IOL, light transmittance to the retina which can interfere by glistenings is not only for a single particle, but also multi-glistenings are counted to evaluate visual quality. If the glistening particles are far from one another then each particle scatters light as if the other particle was not there, and the total light-scattering is simply twice the scattering of an individual particle. However, if the particles are brought closer together so that their surfaces are from one another, then their scattering volumes begin to overlap. Therefore, the total scattering volume from the two glistenings is less than the sum of the two-individual scattering volumes. When the light that enters the overlap volume, light can scatter less efficiently than light that enters a part of the non-overlapping scattering. Therefore, light scattering for group glistening is another problem statement for our research and we follow the above process as single glistening scattering in IOL. Finally, there is no report to evaluate the visibility of IOL with glistenings to solve each of the above problems.

1.3 Research Vision, Purpose and Objectives

The purpose of this study is to evaluate the visibility function of IOL with glistenings from the optical model. In this research, the proposed model study the characteristics of glistenings which are from the lab under temperature changes, calculate the light scattering from multiple light scattering theory and simulate the light transmission to the retina. Moreover, the most important approach of this research considers visual function evaluation from human activities such as driving at night, studying, and walking. Although light scattering is measured from different approaches, there is no research of light scattering effects differs depending upon the human activities. Therefore, this research proposed

the optical model which is intended to evaluate the visibility of intraocular lens with the glistening but cost-effective and accurate methods are also applied for light scattering.

1.4 Dissertation Scope and Outline

The scope of this research is lied on small reflections of light by glistenings that cause forward light scattering in IOL. Glare is the result of forward light scattering and interferes in daily activities of humans. There are several research from clinical studies that investigate the correlation between glistenings and forward light scatter problems. However, there are no findings that visual functions such as disability glare, human activities, and light scattering conditions which can affect the vision quality of human.

In this research, we develop the optical model for the visibility evaluation of IOL from multiple light scattering T-matrix methods. However, this optical model considers the important facts to overcome the real problems which are not yet developed by the previous studies. For this purpose, the flow of this dissertation is outlined as the following Figure 1.2 and each title of the columns is explained briefly.

- Basically, this research is conducted from information science point of view combining with optics to simulate how electric fields are scattered according to the properties of glistenings. Therefore, glistening characteristics are important parameters to calculate the total electric field. Many research reports that glistening can be different size, numbers, shapes, and refractive index which can affect light scattering. Since IOL images from patients have limited resolution to identify the characteristics of glistenings and thus, glistenings are generated in the laboratory with different temperature setting as human body temperature changes. The details are explained in section 3.7.

- Image analysis can help to identify glistening characteristics in IOL and captured with a microscope. From this step, properties of glistenings are received to calculate the light scattering of IOL for the next step in chapter 4.

- Light transmission through IOL to the retina is calculated from electromagnetic light scattering theory and described in chapter 5.

- Visual function is evaluated with one problem of glistenings called glare. For this purpose, straylight value is calculated and evaluated lens quality as chapter 6.

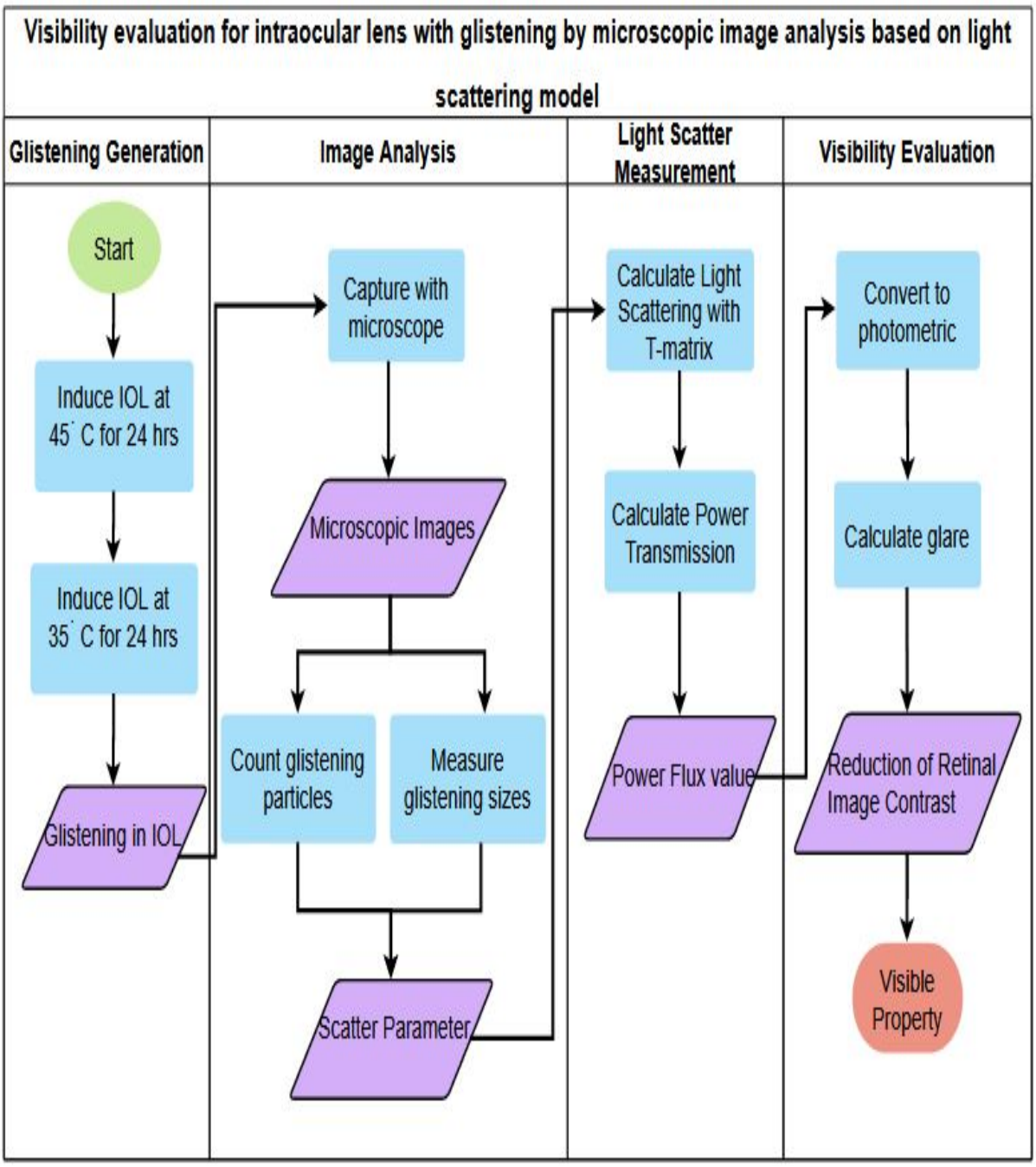

Figure 1.2: Block Diagram of Visibility evaluation for intraocular lens with glistenings by microscopic image analysis based on light scattering model

Chapter 2

Related Works

Today's cataract surgery implant an intraocular lens (IOL) in the capsular bag inside the eyes. There are different types of IOLs that can be used during cataract surgery for different purposes, such as monofocal, multifocal, accommodating, and toric designs. Moreover, various IOL material and designs can be available today, such as hydrophobic acrylic, hydrophilic acrylic, silicone, and polymethylmethacrylate materials; aspheric and nonaspheric, anterior chamber and posterior chamber, one-piece or three-piece, and in-the-bag or sulcus-fixated designs. However, temperature changes between the human body and the manufacturing process cause glistening which accumulates fluid as microvacuoles in IOL. These glistenings are visible through slit-lamp examination since the refractive index difference between that of microvacuoles and IOL materials makes the optical effect. As a result, the differences in refractive indices cause redirection of light and light scattering. Since this research aims to evaluate the vision quality from IOL with glistening, this chapter will firstly discuss available methods to assess the aspects of quality of vision. Many clinical reports investigated the impact of glistenings in intraocular lenses on visual functions such as contrast sensitivity (CS) and visual acuity (VA). However, these findings reported no common descriptions for the effect of glistenings on measured visual quality. Moreover, the study of light scattering in IOL with glistenings can be found in two different methods: Clinical Studies and Mathematical studies. In clinical method, methods of measuring can be subdivided into two categories: the optical in vitro and the optical in vivo in which the former refers to work in a whole living organism, and the latter means performing outside of a living organism.

2.1 Clinical studies

Clinical studies mean that glistenings are observed by using clinical equipment to measure light scattering and evaluate visual function from vivo or vitro methods. The first research is combined of vivo and vitro study because Werner et.al (2016) evaluated forward light scattering and straylight in hydrophobic acrylic IOL which is removed from cadaver eyes. The significance of this research, subsurface nanoglistening is also basically considered and evaluated the impact on optical quality by using a scatterometer to measure forward light scattering and straylight values at different angles were calculated. Furthermore, a scheimpflug camera is used to measure back-scatter and the light transmittance with a spectrophotometer(Lambda 35 UV-VIS) to confirm validate the result. The following Figure 2.1 and Figure 2.2 are scheimpflug camera and spectrophotometer(Lambda 35

UV-VIS) to light scattering in IOL. However, the result concluded that straylight in hydrophobic IOLs from subsurface nanoglistenings would not affect on visual impairments. [21]

Figure 2.1: Scheimplfug camera to measure back-scattering [22]

Figure 2.2: Light transmittance measurement with spectrophotmeter [23]

Secondly, Mo¨nestam et.al (2011) researched with vivo method by studying from patients who had cataract surgery 10 years previously. This research has cooperated with 103 patients who had phacoemulsification with implantation of Acrysof MA60BM IOLs. The purpose is to investigate the impact on visual function from light scattering and glistenings in intraocular lenses from the patients who had experienced with the specified period on eyes. At first, patients were evaluated with best-corrected visual acuity (VA),

and low contrast visual acuity (LCVA). For the purpose of light scattering measurement from IOL, Scheimpflug photography was applied and the degree of glistenings is also defined with slit-lamp. From this research, patients who operated 10 years previously had severe glistenings and a high level of light scattering from their intraocular lenses.[14]

The next vivo clinical research is from Bradley et.al (2015) and investigated intraocular glistenings that have an impact on light scatter and visual function depending on glistening size. This research studied in Pseudophakic patients with visual acuity no worse than 0.02 logMAR and no ocular pathology. Formerly, all IOLs were photographed, and glistenings were analyzed for size and density. Then, the measurement for logMAR corrected distance visual acuity (CDVA), mesopic 10% contrast logMAR CDVA with and without glare is performed, and straylight are assessed by a straylight meter(C Quant log). Figure 2.3 shows the C-Quant device to measure light scattering. To summarize, this research concluded with the age of the IOL which can affect on the glistening size and visual parameters.

Figure 2.3: C-Quant device to measure light scattering [24]

Next, Labus et.al (2016) observed light scattering for glistenings from vitro study. Firstly, glistenings were generated in 7 Acrysof IOLs in the laboratory by changing different temperatures from 37°C to 60°C in a balanced salt solution and cooled to room temperature. The objective of this research is to assess light scattering from intraocular lenses (IOLs) and create a model for predicting glistening effects on straylight. Then, the glistenings were analyzed with a microscope. Therefore, light scattering from the IOLs was experimented and assessed by using a straylight meter (C-Quant) with different scatter angles such as a 2.5-degree and 7.0-degree scatter angle. Then, a model in which the correlation between straylight increase and the total number and area of glistenings was proposed. But, this research is combined the mathematical method and clinical method because results were compared to the Mie theory.[12]

As the last vitro research, Weindler et.al(2019) observed the effect of glistenings on the optical quality of a hydrophobic acrylic intraocular lens. However, this research also used laboratory-induced glistening and experimented to study light scattering. Basically,

image analysis of light-microscopy photographs is applied to learn the number and size of glistenings. In addition, grades are also identified from image analysis which is based on glistening number per mm2. Grade 0 to 4 are reported such as grade 0 (none), grade 1 (1-100), grade 2 (101-200), grade 3 (201-500) and grade 4 (more than 500). For the purpose of evaluating the impact of glistenings on image quality, an optical bench test was employed to measure each IOL's modulation transfer function (MTF) and Strehl ratio. As a result, the number of glistenings(below grade 3) had no effect on the image quality. However, image quality degrading in the MTF and the Strehl ratio were observed in grade 4 but there is no significant effect which can disturb the visual quality.[13]

Summary

All the research which is described from the above reports the results according to their main purposes, but there is some deficiency from clinical studies. As a summary, light scattering from glistenings has been assessed in vivo using Scheimpflug photography for backward scattering or C-Quant straylight meter (Oculus Optikgera te GmbH, Wetzlar, Germany) for forward scattering [25][26]. Although those studies showed the result, some of the research conditions are created to achieve the research goal. For example, glistenings that had developed naturally in the human eye and measured in a laboratory setting have shown strong scattering effects[27][28]. This research combined vivo experiments into vitro settings. Moreover, straylight measurement from vitro–induced glistenings was assessed with a modified straylight meter. Despite that study demonstrated the relationship between a straylight and the number of glistenings, scattering effects will differ between various materials of IOLs. Therefore, clinical research must consider human conditions after implantation even though the experiments are based on vitro methods. IOL materials can produce different scattering effects and thus, those equipment are required to test for all human conditions with different IOL types. In our research, we evaluate the visibility of IOL from the disability glare which is caused by glistenings. An intraocular lens with a large number of glistenings causes disability glare at night and when looking towards the light in the daytime. Such an affected lens may also interfere with a person's ability to drive safely at night. Therefore, the clinical studies are still needed some improvements to satisfy human implanted conditions and glare measurements.

2.2 Mathematical studies

Many research is not found in light scattering problems from mathematical studies. Mathematical studies mean that the effect of glistenings in IOL is studied from light scattering theories and applied with different simulation software. The first research of mathematical study use ray tracing software in an eye model. The purpose of this research is to evaluate the impact of light scatter from glistenings in pseudophakic eyes and thus, mathematical modeling and simulation are operated. As a first step, the pseudophakic eye model was constructed in Zemax using the Arizona eye model as the basis. Then, Mie scattering theory was applied to calculate the intensity and direction of light scattering for spherical-shaped glistening in an intraocular lens. Additionally, the modeling and evaluation of light scattering were observed and modulation transfer function (MTF) was performed for different glistenings with various sizes and density under scotopic, mesopic,

and photopic conditions. As a result of the simulation, increasing the density of glistenings shows the significant drop in the MTF of the IOL and the pseudophakic eye.[7]

In Mooren's research[16], laboratory-induced glistenings were generated first and then the light scatter contribution induced by microvacuoles was measured as a function of both angle and extinction and was verified by calculations using Mie theory. For this reason, four IOL types are used to measure the microvacuole particle size distribution and particle volume density by using confocal light microscopy and dark field microscopy, and the corresponding extinction coefficient γ was determined. The final output of this research summarized as IOLs with significant glistenings shows stray light levels higher than that of a healthy 20-years-old crystalline lens.

Next, this research studied for the specific size glistenings called subsurface nano glistenings which have described 3 sizes in experiments such as 100 nm, 150 nm, and 200 nm. Since the object of this study is to determine whether subsurface nanoglistening in hydrophobic acrylic intraocular lenses (IOL) decline visual performance. Therefore, the effect of subsurface nanoglistenings was simulated using optical design software Lighttools and Code V with the Liou-Brenann model eye and an acrylic IOL. As a result, subsurface nanoglistenings increased forward scattering slightly and reduced irradiance but significantly diminished retinal image. The effect of subsurface nanoglistenings on visual function in the absence of severe retinal disease was minimal.

Summary

The above mathematical studies are based on lab-induced microvacuoles and applied mathematical theories to evaluate the light scattering problem. Mie light scattering model is used and the results are simulated by commercial tools such as Zemax, Lighhtools, and CodeV. However, light scattering from glistenings in IOL is not calculated from the multiple light scattering approach since glistenings are densely located in IOL. Although eye-models and lab-induced glistenings have experimented from these studies, human activities are not considered for assigning wavelengths in light scattering evaluations such as night time driving or studying. In fact, human eyes have photoreceptors called rod and cones which are providing the vision to the eyes. However, rods provide vision during dim light or night also known as scotopic vision, whereas cones provide vision during day time or at bright light also known as photopic vision. Depending upon the activities of humans, light levels are different. Moreover, rod and cone cells have sensitive wavelengths. For example, the rod is sensitive at 498 nm and is insensitive to wavelengths higher than 640 nm. In cone cells, the wavelength of approximately 420 nm, 534 nm, and 563 nm and the sensitivity may raise to provide vision over the visible spectrum [29]. However, these lighting conditions and wavelengths are not considered in the above literature.

Chapter 3

Glistening in Intraocular Lens

3.1 Anatomy of the human eyes

Human eyes are the main sense organ capable of receiving visual images, which are then carried to the brain.[30]. The eye has many functions to produce a clear vision.

- The sclera, white part of the eye and outer layer which protects the eyeball.
- The pupil, black dot at the center of the eye, and light can enter the eye through it.
- The iris, coloured part of the eye, surrounds the pupil. The main task of the iris is to control the light which enters the eye by changing the size of the pupil.
- The cornea, a clear window at the front of the eye, covers the iris and the pupil.
- A clear lens, located behind the pupil, acts like a camera lens by focusing light onto the retina at the back of the eye.
- The retina is a light-sensitive inner lining at the back of the eye. Ten different layers of cells work together in the retina to detect light and turn it into electrical impulses.

Anatomy of the eye is important to understand where cataract occurs and how and when the surgery is required to implant IOL where glistenings have been found. In Figure 3.1, Anatomy of the human eyes with cataracts can be seen when light passes through the lens. Clouded vision can be caused by cataracts and can interfere in daily activities such as driving and reading. Although several reasons for eye conditions can cause cataract, aging or injury changes the tissue in the lens of the eyes can develop the cataract more than others. Therefore, the common treatment to cataract is the surgical removal of the lens and implanted with IOL. In the next section, IOL implantation is described.

3.2 IOL implantation

The human eye has a lens that focuses light onto the retina and then sends it to the brain. Therefore, the lens is a key refractive element of the eye to see images of the visual world onto the retina. But cataract makes the lens to be cloudy and look blurry. Hence, cataract surgery removes the cloudy lens and replaces with IOL to correct vision problems. In cataract surgery, the lens inside the eye that has become cloudy is removed and replaced

with an artificial lens (called an intraocular lens, or IOL) to restore clear vision. In fact, the intraocular lens (or IOL) is an artificial lens for the eye and helps light to enter after the natural lens is removed in cataract surgery. However, there are different types of IOL materials which can select from plastic, silicone, or acrylic. Moreover, they are available in a variety of focusing power: monofocals, aspheric, multifocal, accommodating, and toric.

- Monofocal IOL: This is the most common type of IOL which is used to remove the eye's natural lens after cataract surgery. This type of IOL can stretch or bend to help the eye focus. But, this IOL focus at one fixed distance for close, medium, or distance vision. Basically, patients are set this type of IOL for clear distance vision but, eyeglasses are still required for reading or close work.

- Multifocal IOL: This lens is similar to the function of glasses with bifocal lenses which can help to see near and far. Moreover, this IOL provides several different focusing distances within the same lens, but it is appropriate for the patients who implant in both of the eyes rather than just one.

- Accommodating IOL: This IOL is flexible and works as a natural lens and focuses can be more than one distance. In fact, the shape of the lens is not changed, but the ciliary muscle in which IOL is accommodated can move back or forth to change the focal point for different distances.

- Toric IOL: Toric IOLs are used to correct astigmatism which is a common vision problem before and after cataract surgery. Astigmatism means that the curvature of the cornea is irregular and causes light to focus at multiple points in the eye instead of focusing only at one point on the retina and vision can be blurry. This lens helps to lessen astigmatism and thus glasses are not needed to wear after surgery.

3.3 Scatter in IOL

The degrading of vision quality by glistenings in IOL related to increased forward light and results in retinal straylight. Figure 3.2 shows how light is scattered inside the eyes. In addition, retinal straylight is correlated to other vision complaints such as glare, halos, color, and contrast loss. Scatter in the IOL can be categorized into two types which are based on the direction of the scattering: forward scattering and backward scattering.

- Forward scatter is defined as the total amount of light scattered towards the retina (angular distribution between 0^{o} and 180^{o}), resulting in a veiling illuminance superimposed upon the retinal image and causing a reduction in contrast.[18] This situation leads to a variety of complaints, such as glare. In a clinical experiment, forward light scattering is measured by using a double-pass imaging technique or with a straylight meter.

- Backward scatter on the other hand is defined as the total amount of light scattered back towards the anterior chamber (angular distribution between 180^{o} and 360^{o}), reducing the amount of light reaching the retina. Clinically, backward light scattering can be studied by slit-lamp examination or the use of a Scheimpflug camera.

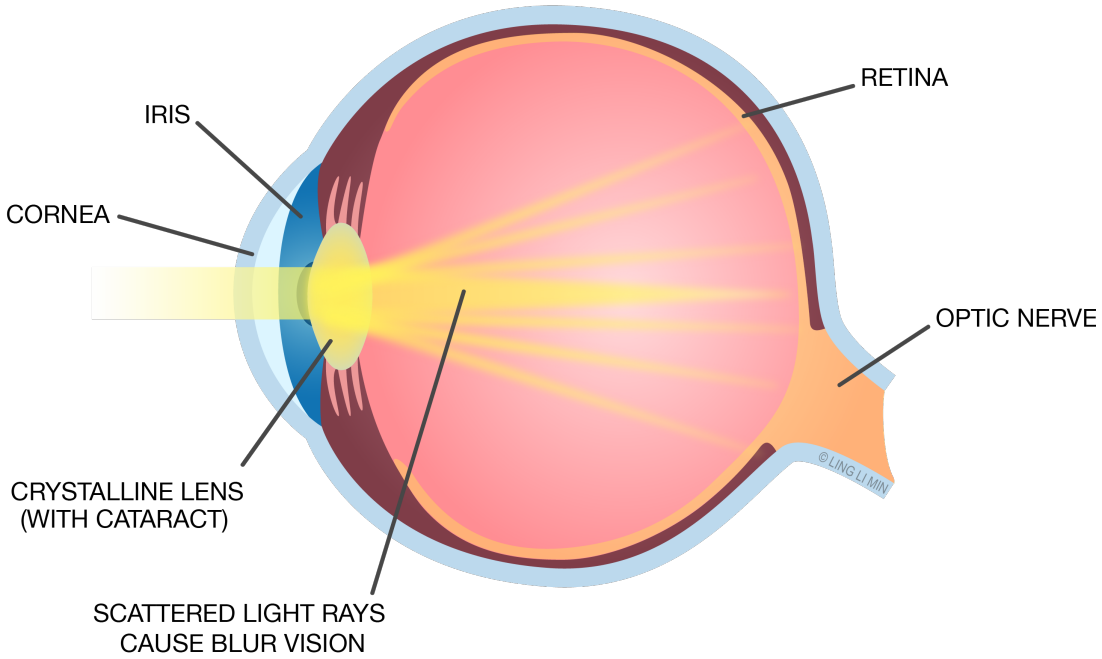

Figure 3.1: Anatomy of the human eyes with cataract [31]

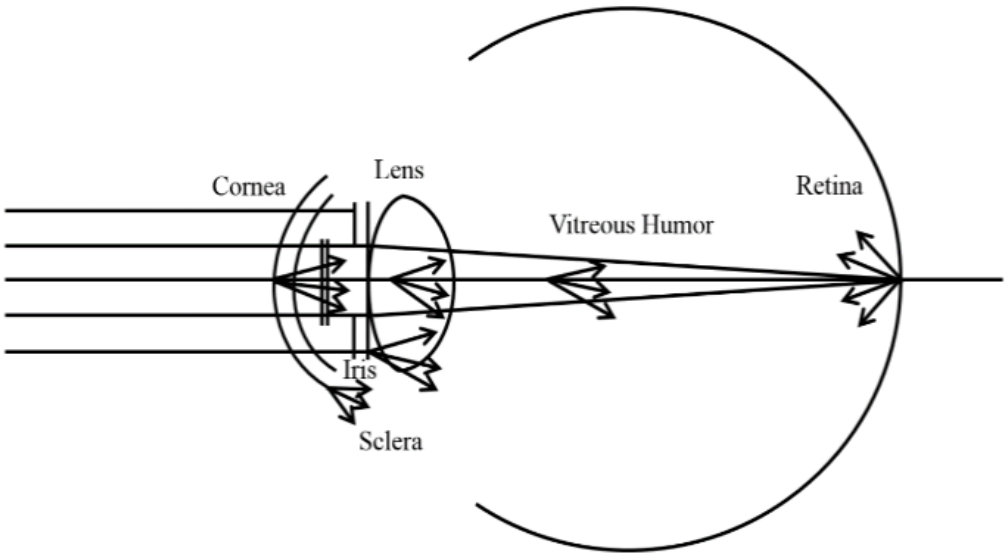

Figure 3.2: Scattering in human eyes [32]

3.4 Electromagnetic Scattering

Light scattering can be defined as the redirection of light in which an electromagnetic (EM) wave (i.e. an incident light ray) encounters an obstacle such as the glistening particle in this research. When the EM wave interacts with the discrete particle, the electron orbits within the particle's constituent molecules are perturbed periodically with the same frequency as the electric field of the incident wave. The oscillation or perturbation of the electron cloud results in a periodic separation of charge within the molecule, which is called an induced dipole moment. The oscillating induced dipole moment is manifest as a source of EM radiation, thereby resulting in scattered light. The majority of light scattered by the particle is emitted at the identical frequency of the incident light, a process referred to as elastic scattering. In summary, the above phenomenon describe the process of light scattering as a complex interaction between the incident EM wave and the molecular/atomic structure of the scattering object; hence light scattering is not simply a matter of incident photons or EM waves "bouncing" off the surface of an encountered object.

Formal light scattering theory may be categorized in terms of two theoretical frameworks. One is the theory of Rayleigh scattering (after Lord Rayleigh) that is, strictly speaking as originally formulated, applicable to small, dielectric (non-absorbing), spherical particles. The second is the theory of Mie scattering (after Gustav Mie) that encompasses the general spherical scattering solution (absorbing or non-absorbing) without a particular bound on particle size. Accordingly, Mie scattering theory has no size limitations and converges to the limit of geometric optics for large particles. Mie theory, therefore, may be used for describing most spherical particle scattering systems, including Rayleigh scattering. However, Rayleigh scattering theory is generally preferred if applicable, due to the complexity of the Mie scattering formulation. In this research, glistening particles are assumed as spheres and thus, mie scattering is relevant to apply but multiple scattering problem is also considered. The difference between Mie scattering and Rayleigh scattering can be seen in Figure 3.3. Therefore, T-Matrix approach is suitable for this research and discusses the theory in Chapter 5.

Theory of Rayleigh light scattering

This theory was initiated by Lord Rayleigh from the research on scattering from small particles and is applicable to small, spherical particles. However, Rayleigh scattering is more effective at short wavelengths. For light scatter measurement, forward scatter equals backward scatter in Rayleigh theory.

Theory of Mie light scattering

Mie scattering has no particle size definition and moreover, this type of scattering is not depend on the wavelength and forward scatter does not equal back scatter. In human eyes, normal eyes or cataract-eyes, scattering is not wavelength dependent, and thus Mie scattering is more convenient to calculate glare[33].

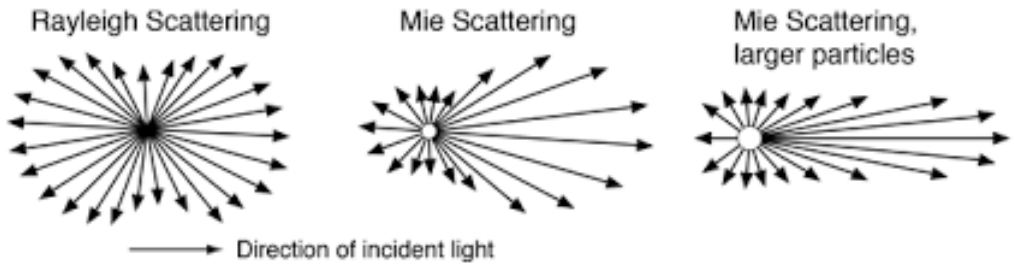

Figure 3.3: The difference between Mie scattering and Rayleigh scattering [34]

3.5 Measurement of Visibility

Vision is composed of many visual functions and thus, quality of vision and perceived reading ability in patients is important to be tested and measured. Vision can be measured by many different tests which are used in clinics or hospitals. Generally, visual impairments in cataract are caused by intraocular forward light scatter[35] and likewise, in glistenings. However, the common visual function tests that are performed for assessing the visual function of cataract patients: visual acuity(VA), contrast sensitivity (CS), and glare disability (GD). Therefore, visual functions for glistenings are also assessed by these three tests. Although visual acuity (VA) is the conventional test of visual function in patients with cataracts, some good VA patients complain of poor vision. Hence, other tests of visual function such as contrast sensitivity (CS) are also evaluated to assess the quality of vision and the following sections will discuss the details of each of the tests.

3.5.1 Visual Acuity

Visual acuity (VA) is a measure of the ability of the eye to distinguish shapes and the details of objects from a specific distance. The result of Visual acuity value is described by a fraction (for example, 20/20). Visual acuity 20/20 vision is normal, otherwise, corrective eyeglasses, contact lenses, or surgery are needed to have a clear vision. In fact, visual acuity is tested monocularly with high contrast which means black letters are written on a white back. However, the patient's eyes are tested one at a time while the other eye is covered. For this purpose, doctors use a standard chart or a viewing device with smaller letters. There are two common tests which is used in VA: (1) Snellen and (2)Trumbling E.

Snellen

The Snellen test uses a chart of letters or symbols which are arranged in different sizes by rows and columns. Viewed from specific distance away(for example, 14 or 20m), the test examine how patients can distinguish the letters by reading out to the doctor while one eye is covered. This process will repeat and read smaller and smaller letters until patients can no longer accurately distinguish letters. Figure 3.4 shows Snellen chart for visual acuity testing.

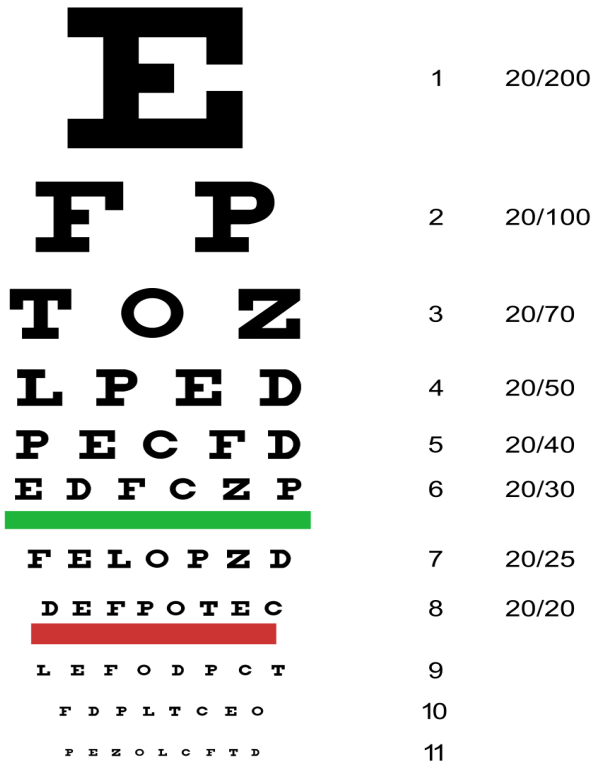

Figure 3.4: Snellen chart for visual acuity testing [36]

Trumbling E

The trumbling E test uses the direction of the letter "E" is facing. In this test, patients look at the letter on a chart, directions of the letters are examined such as up, down, left, or right. This test can help to determine the patients need vision correction because the doctors change the lens until the clear vision to see the chart. Figure 3.5 shows trumbling E chart for visual acuity testing.

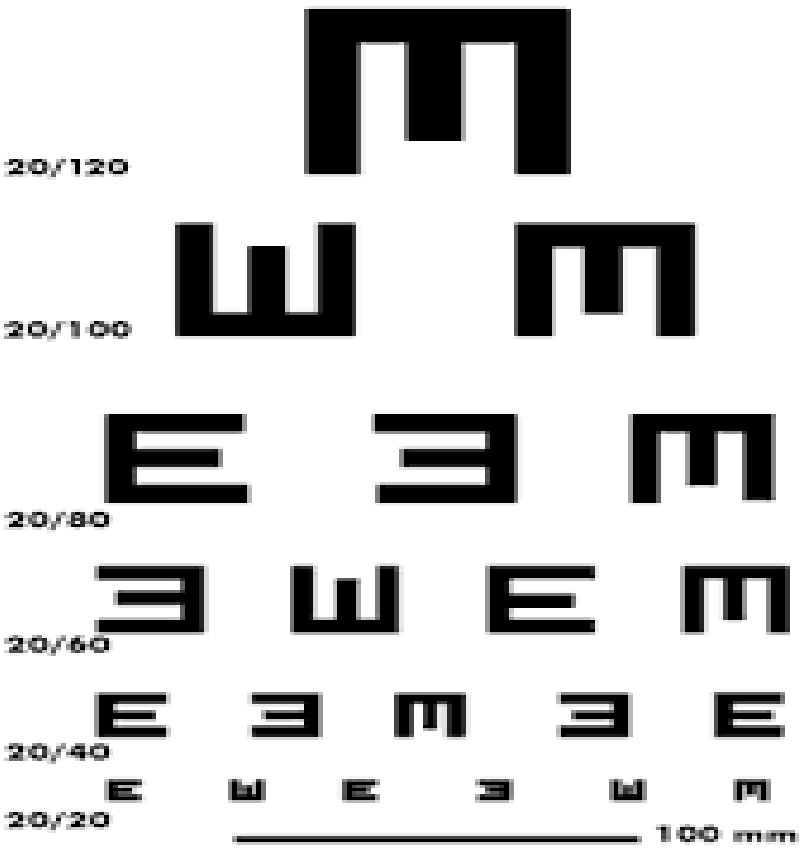

Figure 3.5: Trumbling E chart for visual acuity testing [37]

3.5.2 Contrast Sensitivity

Contrast sensitivity measures the ability to distinguish between an object and its background using low contrast letters. However, cataracts can increase intraocular light scatter, and thus it can decrease retinal image contrast which affects contrast sensitivity. In cataract patients, contrast sensitivity is affected more than visual acuity because higher-order aberrations are significantly correlated with contrast sensitivity at intermediate to higher spatial frequencies in eyes with cataracts. However, contrast sensitivity is important to measure visual function because the contrast between objects and background is reduced in situations of low light. For example, good contrast sensitivity is required for safety while driving at night. To test the contrast sensitivity, Pelli Robson contrast sensitivity chart is used in the examination of the eyes. Pelli Robson chart for contrast sensitivity testing is depicted in Figure 3.6.

Figure 3.6: Pelli Robson chart for contrast sensitivity testing [38]

3.5.3 Disability glare

Patients with cataracts complain of glare, for example from bright sunlight or car headlights. In addition, this glare can affect disabling more than a moderate drop in visual acuity. However, previous studies reported that glare disability with cataracts does not correlate with visual acuity[35][39][40]. Although patients suffer significant glare disability, visual acuity can be good. Therefore, disability glare is important to measure the quality of vision. Disability glare means the loss of retinal image contrast by cause of intraocular light scatter and this is called forward light scatter. Oppositely, backscatter is the diffusion of light which reflected out of the eye and can be seen by an external observer. Light scattering theory can be applied to study the glare by means of two theoretical models and moreover, the brightness acuity test (BAT) can also perform to simulate glare from a light source.

3.6 Characteristics of glistenings

In recent years, there are several studies related to glistening characteristics and methods to assess glistenings in IOL. Glistenings can be found with different characteristics such as size, number, and reflective indices which depend on the material of the lens. In fact, glistenings are small water inclusions in IOL and thus, the different sizes of glistenings can be found. According to previous studies, glistenings has been reported with the diameter

range from 10 to 20 µm by Dogru et al. (2000) [6]. However, the different size of glistenings have been found by DeHoog et al. (2014) and experimented with 2 to 200 µm in diameter [7] but Henriksen et al (2015) presented as two groups: 6 to 25 µm or greater than 25 µm [8]. Recently, the size of glistening is significantly varied and observed by Takahashi et al. (2015) that the size range is between 1 µm and 120 µm [9] but the optical simulation in that research was implemented by three different sizes: 100 nm, 150 nm, and 200 nm.

The number of glistening in IOL is also an important factor for grading glistening. In fact, glistenings are graded in the intraocular lens by clinicians through the slit lamp. They manually counted the number of glistenings and report as different grades. Therefore, several studies described grading by the number of glistenings present in IOL. Firstly, three grades of glistenings such as 1 +,2 + , and 3 + have been reported by Dhaliwal et al. (1996) [10]. Moreover, glistening grades are recorded as 0 to 3+ by Wilkins and Olson (2001) in which 0 for no glistenings, 1+ for less than 10, 2+ for 10 to 50, and 3+ for more than 50 [11] . Yet, Cisneros-Lanuza et al. (2007) proposed glistening appearance in IOL and graded 1+ for 10 to 20, 2+ for 20 to 30, 3+ for 30 to 40, and 4+ for more than 40 glistenings [41]. However, glistening numbers are classified and measured per mm2 by Geniusz et al. (2015) where grade 0 (none), grade 1 (1-100), grade 2 (101-200), grade 3 (201-500) and grade 4 (more than 500) [13]. According to previous studies, grading scales can be represented by the occurrence of glistening numbers in IOL, but the common agreement is not found on defining glistening's grading.

The microvacuoles were distributed randomly in the spherical coordinate system of IOL. The refractive indices of glistenings and IOL were assigned to 1.336 and 1.5. Firstly, initial excitation for the simulations is used as a Gaussian beam with a beam waist of 4 µm. The wavelength parameter(λ) is given 550nm because the human eye's visibility wavelength is in the range between 390nm and 720nm. Since there is no standard defining the glistening's grading, the number of glistening in each simulation is grouped as grade 1 (less than 10), grade 2 (10-50), grade 3 (50-100), and grade 4 (100-500).

3.7 Glistening generation

In this experiment, hydrophilic acrylic IOLs was used from Gennext aspheric Foldable IOL which is made from natural yellow material with a special monomer containing the identical chromophore present in the human crystalline lens. Natural Yellow is the first IOL material to incorporate the same UV-A blocking and violet light filtering chromophore that is in the human crystalline lens. The approach, to UV blockers and violet filters is to use nature's own solutions to the problem of protecting the retina from harmful energetic light[42]. The figure of IOL is shown in Figure 3.7 and the specification of the lens are described in the following Table 3.1:

Figure 3.7: Hydrophilic acrylic IOL[43]

Table 3.1: Description of IOL

Lens Model	YSQ FL600ASP
Optic Design	Aspheric/Double Square Edge 1 Biconvex
Optic Diameter	6.0 mm
Overall Length	12.5 mm
HapticAngle	00 , Elastic band design
A-Constant	118.2
Diopter Range	8 to 30 (in 0.5 increment in D+ 18 to 25)
Water Content	25% BENZ

All lenses were extracted from the original packages and immersed in saline solution in the water bulb. According to the previous studies [12][13][44][16], glistening generation is processed between two temperature change within 48 hours. For this purpose, EC water bath model(EW-100K) is used in which the temperature setting is available from 0°C to 100C. Firstly, microvacuoles were induced by taking the IOL from its room temperature environment and placed it into an induction at temperature of 45°C for 24 hours. Then, another temperature is set with 35°C for 24 hours in the water tub. Afterward, the lenses were removed from the oven and measure at room temperature. The densities of induced microvacuoles vary with the time following their removal from the oven. For this reason, restrictions were made with respect to the time points of measurements. The following Figure 3.8 shows how to induce the IOL in the water tub.

Figure 3.8: Induction of IOL to generate microvacuoles

Chapter 4

Image Analysis for glistenings in IOL

IOL images are analyzed to obtain the number and size of glistenings for optical simulation in the next step by using the image processing technique. In the previous chapter, glistenings are generated in the laboratory and discussed at glistening generation in section 3.7. In this research, we employed an open-source library ImageJ[45] for image analysis. Firstly, glistening is detected from microscopic images and analyze the particles according to the following Figure 4.1.

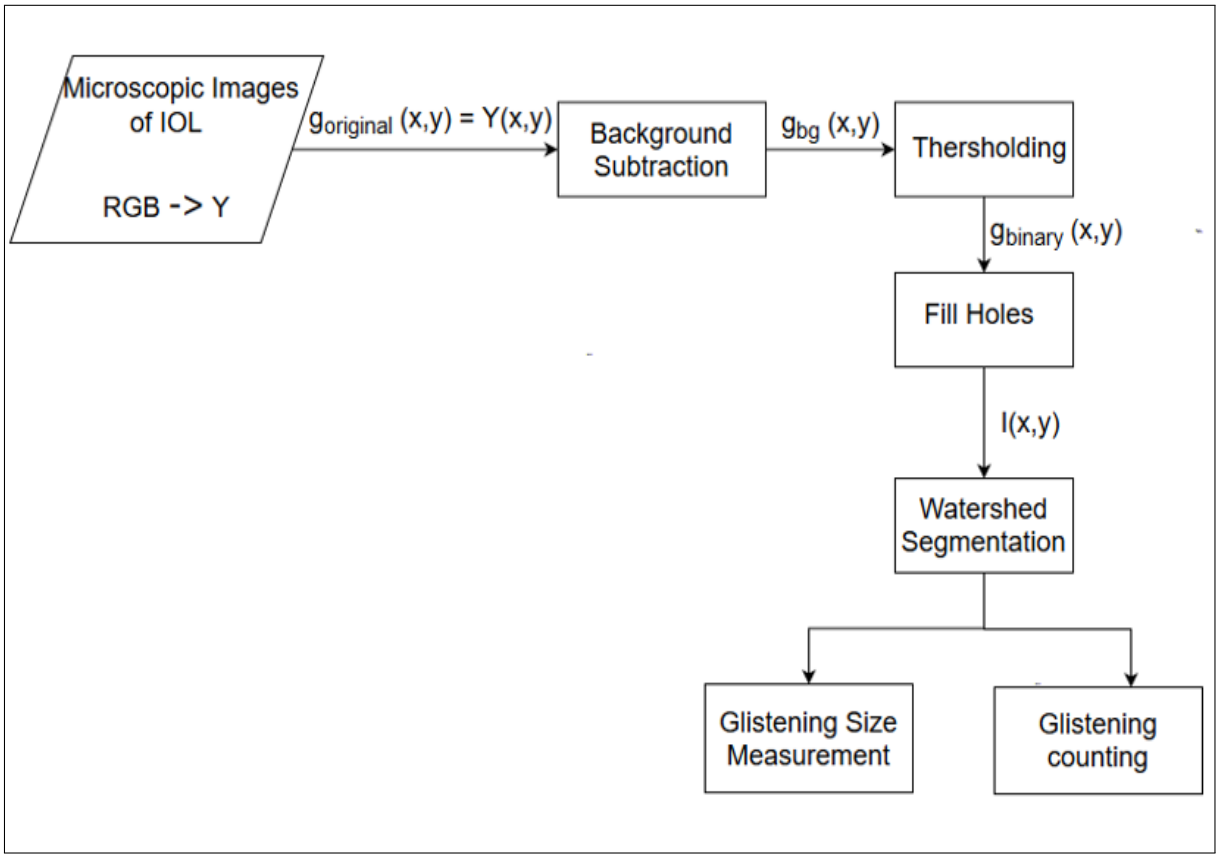

Figure 4.1: Flow chart of Image Analysis

4.1 Microscopic Images of IOL

To calculate light scattering in IOL from microscopic images, lens imaging is performed by confocal microscopy and dark field microscopy. Confocal microscopy has a limited depth of focus in which images were taken throughout the thickness of the lens and then stacked. This kind of microscopy has a small field of view and thus, it is needed for three or more lateral displacements across the lens to capture the complete central optic body. Dark field microscopy is used as the intraocular lens is needed to be retro-illuminated with an annulus of light and thus, a large field of view is the main difference from confocal microscopy[16]. In order to capture glistenings inside the lens, an inverted microscope(Olympus IX73) is used for nano-sized particles or micro-sized particles in which the light source and the "condenser" lens are above the specimen. Figure 4.2 shows the Olympus IX72, an inverted lens for capturing microscopic images. In fact, Olympus IX72 can provide UIS2 optical system and focus 10 mm. Moreover, the observation method is available for Fluorescence (Blue/Green Excitation), Fluorescence (Ultraviolet Excitation), Differential Interference Contrast (DIC), Phase Contrast, bright field. The observation tube is Widefield (FN 22) for tilting binocular and trinocular. The objective is on the bottom and thus, it can focus the light to produce a real image.

Figure 4.2: Lens imaging with microscope

If there are no glistenings for light scatter, the image is black. Otherwise, glistenings can be seen as while particles in a dark background. Next, Image analysis methods are applied to identify the size and number of the microvacuoles from the images for light scatter calculation.

4.1.1 Glistening and Whitening in IOL images

The lab-induced glistenings and whitening are taken by an inverted microscope and shows in Figures 4.3, 4.4, 4.5, and 4.6. IOL images are captured with different magnification to have better result such as 20X, 40X, and 60X.However, microscopic image with 40X magnification(Figure 4.5) is used for the glistening measurement in this experiment. Since

glistenings are very small in microscopic image of IOL, the image is divided into 25 images to be a high performance in image processing algorithm but size of images are the same.

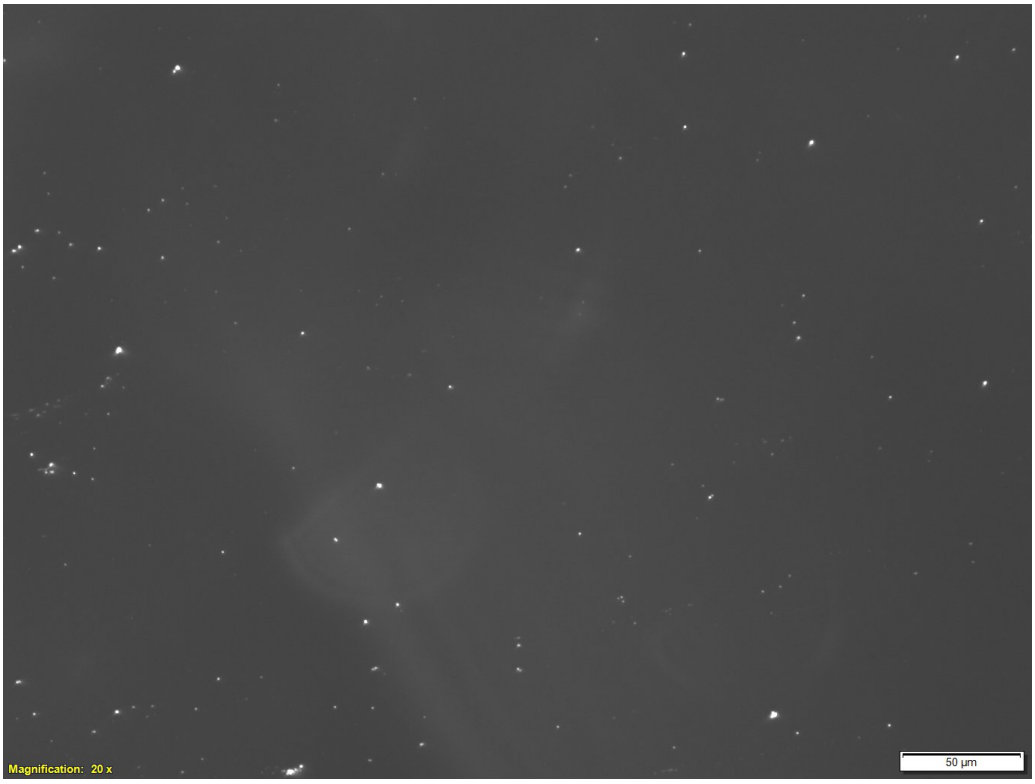

Figure 4.3: Glistening in microscopic image of IOL with 20X magnification

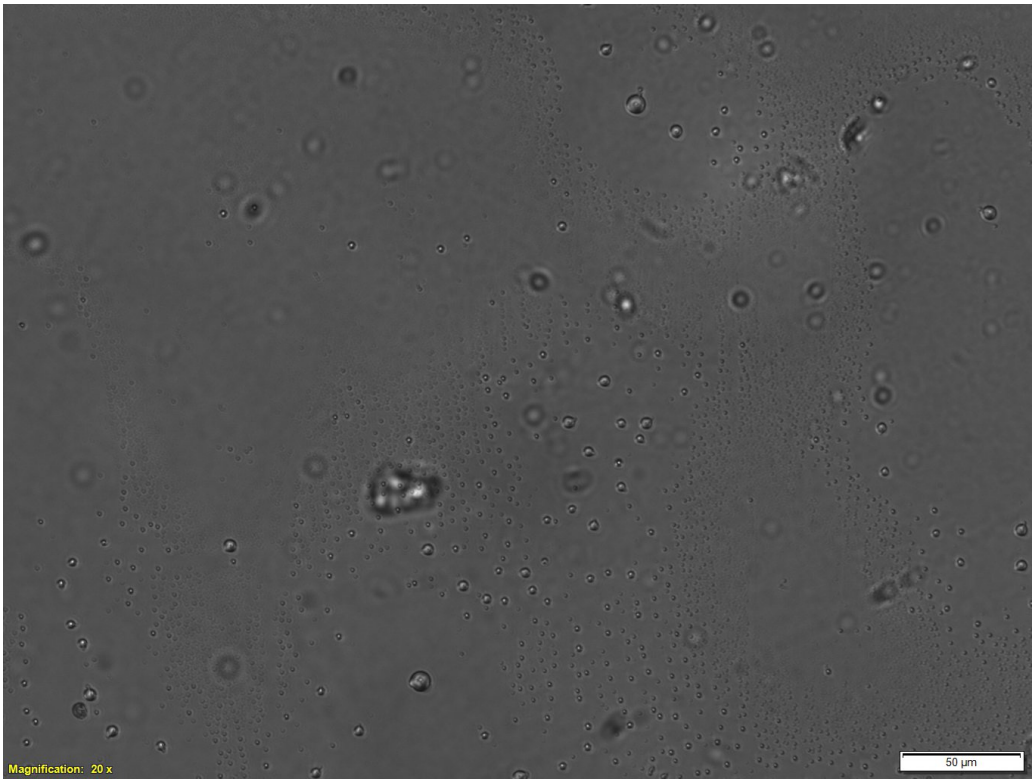

Figure 4.4: Glistening in microscopic image of IOL with 20X magnification

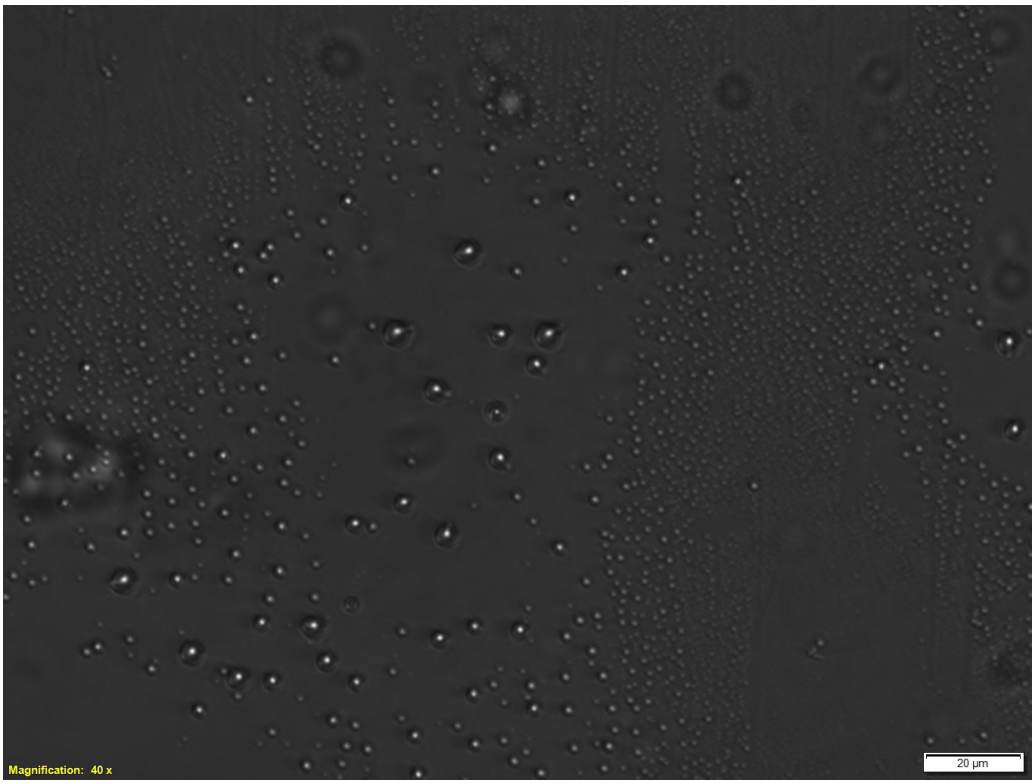

Figure 4.5: Glistening in microscopic image of IOL with 40X magnification

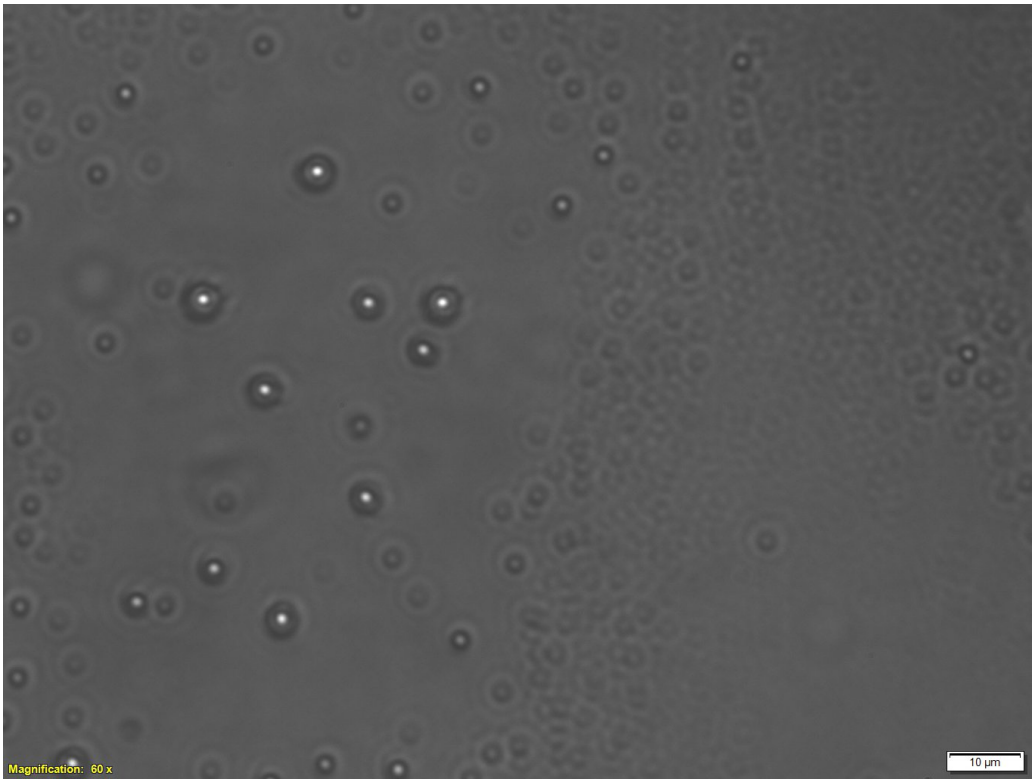

Figure 4.6: Glistening in microscopic image of IOL with 60X magnification

4.2 Background Subtraction

Image preprocessing is performed to adjust images which is applicable for the next step of glistening computation process in IOL. Firstly, the input images are converted into gray-scale 8 bit images. From this gray-scale image, background subtraction is proceeded. Background subtraction is important for an uneven background in the image. In IOL images, glistening are very small and other lighting condition can also have some impacts to distinguish background and foreground and thus, background subtraction is considered based on "rolling ball" algorithm [46]. The algorithm assumes 2D grayscale image has a height dimension defined by the intensity value at every point in the image, then a ball (filtering object) rolls over the image in order to find smooth continuous background. When a ball with a radius sufficiently large not to fall into points moves on this surface, its center generates another surface, whose shape is affected by only general grayscale variations.

The center of the filtering object, a surface from the top of a sphere have a radius(R) which is moved along each scan line of the image. Therefore, the surface is tangent to the image at one or more points with every other point on the surface below the corresponding (x, y) point of the image. Any point either on or below the surface during this process is considered part of the background. The following equation shows that the background subtraction by the rolling ball method:

$$g_{bg}(x, y) = (g_{original}(x, y) + 1)–(C(x, y)–R) \tag{4.1}$$

where $C(x, y)$ is the patch generated by the ball center and R is the ball radius. Figure 4.7 shows a schematic diagram of background subtraction by rolling ball method. In this diagram, the histogram indicates the surface determined by the original grayscale distribution $g_{original}(x, y)$; (1) surface $C(x, y)$, generated by the ball center; (2) surface $(C(x, y)–R)$, determined by the point of the ball contact with the surface $g_{original}(x, y$; (3) $(g_{original}(x, y) + 1)$; and (4) new grayscale distribution with the uniform background $g_{bg}(x, y) = (g_{original}(x, y) + 1)–(C(x, y)–R)$.

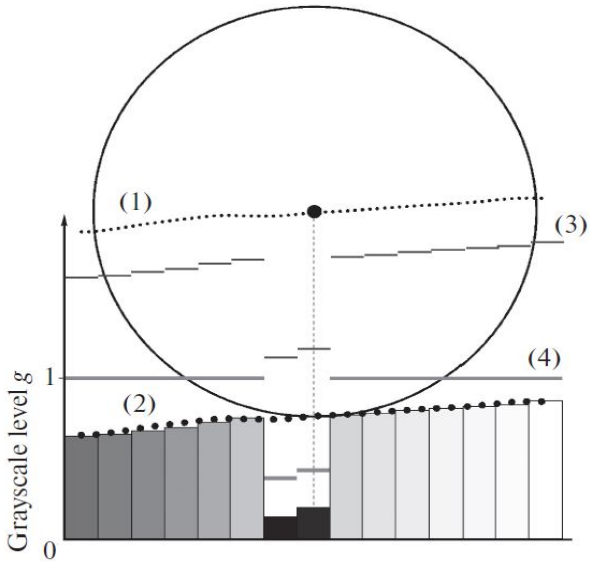

Figure 4.7: Schematic diagram of background subtraction by rolling ball method [47]

Background subtraction with rolling ball algorithm is applied to glistening images in IOL and the result can be seen as Figure 4.8.

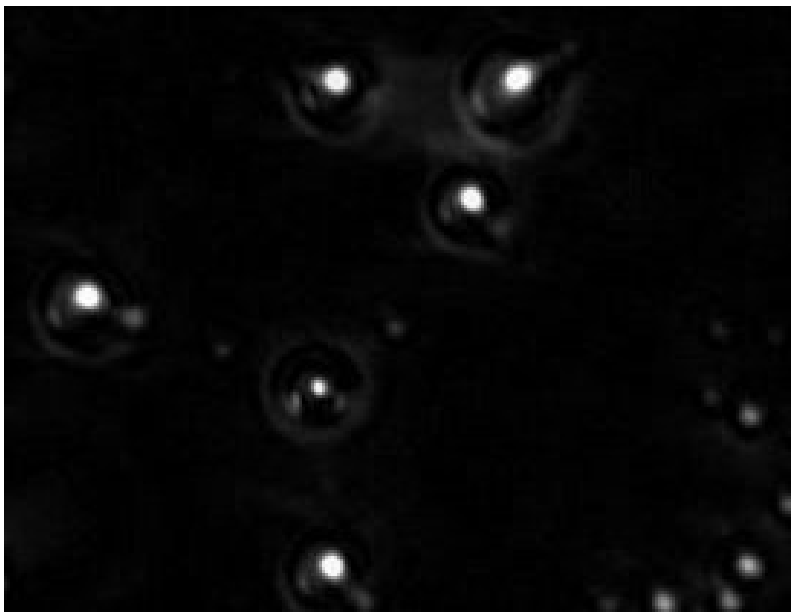

Figure 4.8: Background subtraction in microscopic image of IOL

4.3 Thersholding

Thresholding is the simplest method of image segmentation which can be used to create binary images from grayscale images[48]. Image segmentation means the process of partitioning a digital image into multiple segments (sets of pixels, also known as image objects). The goal of segmentation is to simplify and/or change the representation of an image into something that is more meaningful and easier to analyze [49][48]. Therefore, the outcome of the preprocessed image is feeding to the segmentation stage. Glistening features in IOL image are extracted from the surroundings using a thresholding technique in which all gray levels below the threshold are mapped into black, those levels above are mapped into white, or vice versa.[50]. In this research, the thresholding function is used based on the isodata algorithm [51] and applied in the glistening images.

$$g_{binary}(x, y) = T(g_{bg}(x, y), t) \tag{4.2}$$

where $g_{bg}(x, y)$ is the subtracted background image and T is the thresholding function in which t is defined as threshold value. Therefore, t value is calculated from isodata thresholding. However, the output of Isodata thresholding for microscopic image is shown in Figure 4.9.

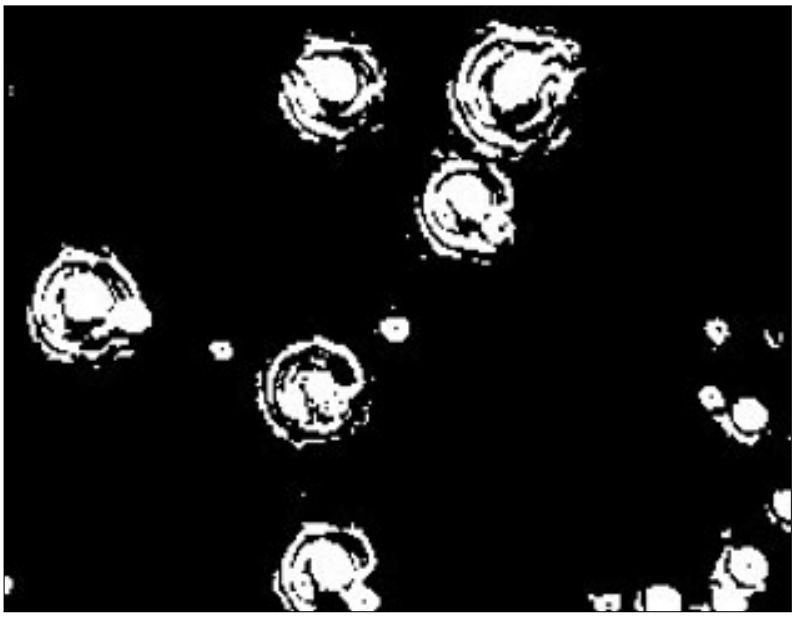

Figure 4.9: Thresholding in microscopic image of IOL

In fact, Isodata theresholding divides the image into objects and background by taking an initial threshold. Firstly, a threshold value t is defined from the range of gray values in the image. Then, the mean of all pixels with a gray value less then or equal to t is calculated as m_L and the mean of all pixels with gray value greater than t are also calculated as m_H. Afterward, the averages from two values are calculated but the threshold value is incremented and the process is repeated until the threshold is larger than the composite average. Thus, Isodata thresholding can be written as:

$$t = \frac{m_L + m_H}{2} \tag{4.3}$$

From the above equation, the value of t is between m_L and m_H and thus, both m_L and m_H are also functions of t. Therefore, the above equation can be transformed into:

$$t = \frac{m_{L(t)} + m_{H(t)}}{2} = m(t) \tag{4.4}$$

where function m is defined. A point t such that $t = m(t)$ is called a fixed point of the function m. Starting from an initial estimate to the fixed point can be found with fixed point iteration:

$$t_{i+1} = m(t_i) \tag{4.5}$$

This process is repeated on the input image until the threshold version remains constant for further iterations.

4.4 Fill Holes

After thresholding of microscopic IOL images, we fill all the holes of every detected edge by filling the holes. In fact, the image contains foreground objects surrounded by background regions. However, some imperfections in the binary image are set of background regions lying completely within the foreground regions due to imperfection in the binary

conversion identified by thresholding. Therefore, these holes are filled in glistenings of microscopic IOL images and shows as Figure 4.10.

$$I(x, y) = max(g_{binary}, O(C(O(g_{binary})))) \tag{4.6}$$

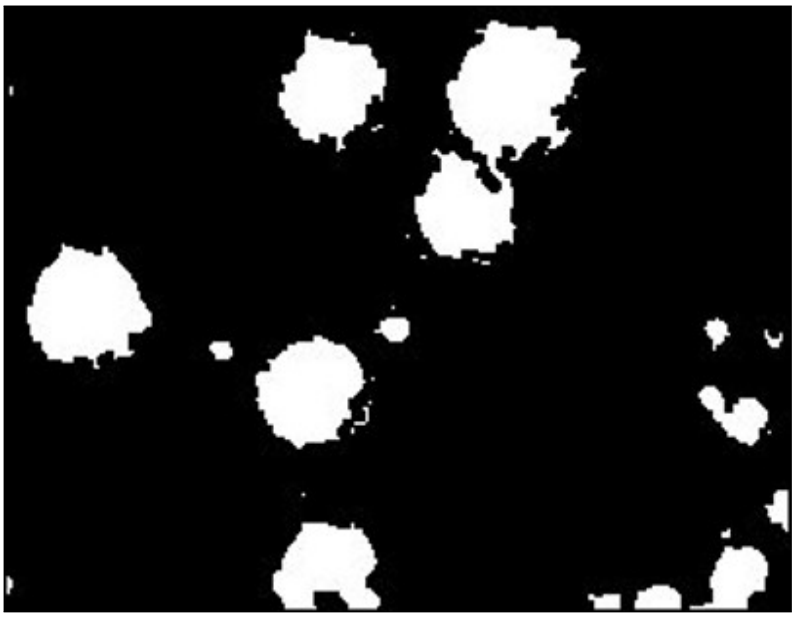

Figure 4.10: Filling holes in microscopic image of IOL

4.5 Separation of Overlapping objects

Watershed segmentation is applied to binary IOL images because some of the glistening particles are closed and touched each other after filling holes. Watershed segmentation algorithm based on mathematical morphology is a well known image segmentation approach[52][53]. This method is based on the approach of geography in which pixel values are in the altitude while other local minimum values and its surrounding regions represent basins. Firstly, the algorithm assumes that the work flow as filling water to the basin, and two or more basins water meet as dam. That is called watershed line in which the basins are located between the boundaries. This process will finish when all basins have surrounded the dam. After watershed segmentation has applied in IOL images, glistenings segmentation and overlapping parts are separated and easier to identify for counting in the next step. Figure 4.11 shows how the watershed algorithm separates the touching glistening particles.

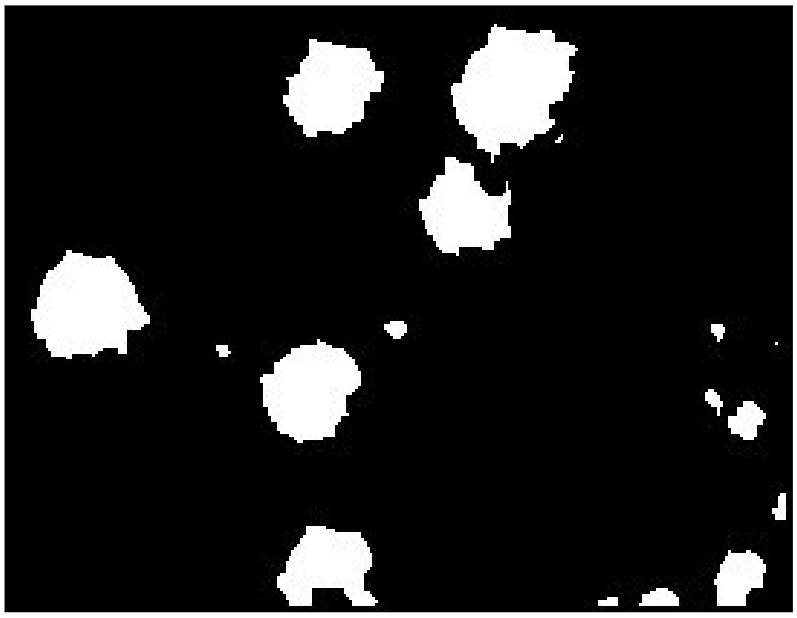

Figure 4.11: Overlapping parts are separated by watershed algorithm

4.6 Glistening counting

The main purpose of image analysis is to know the number and size of glistening for light scatter calculation from lab-induced glistenings. Therefore, all segmented images are automatically counted by image processing. In this step, we obtain the information of each glistening by outlining the numbers. Figure 4.12 shows how automatic glistening counting from the segmented image of IOL.

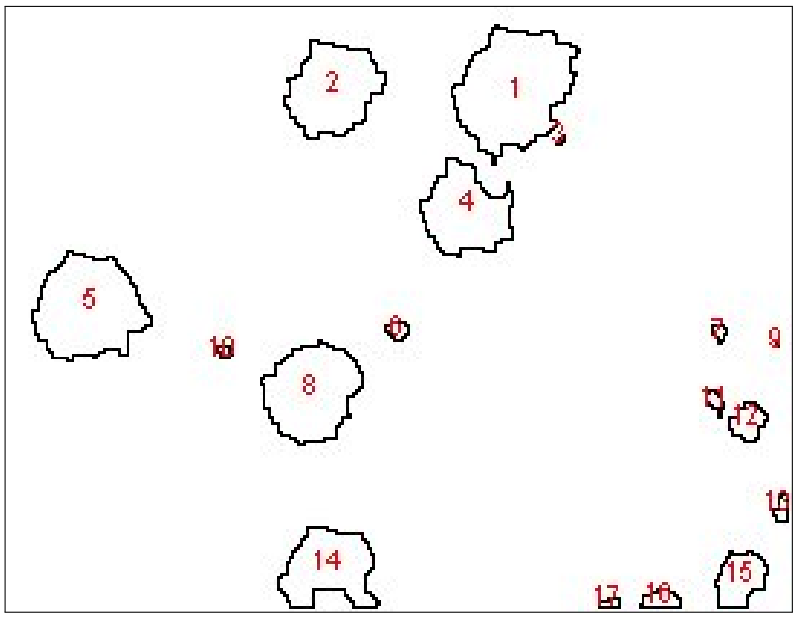

Figure 4.12: Glistening counting in microscopic image of IOL

4.7 Glistening measurements

The next result of automatic glistening counting is the size of glistenings. Since the area of glistening particles is computed, the diameter of each particles is calculated again by the following equations. However, we assume all the particles are spheres for light scattering calculation in the next chapter.

$$diameter = 2 * \sqrt{area/\Pi} \tag{4.7}$$

4.8 Result of Image Analysis

The result of induced microvacuoles from IOL is analyzed by image analysis. From this analysis, the size of glistening and the number of glistening can be achieved. The following Figure 4.13 shows the number and size of glistening from this experiment. Although size is one of the parameters to calculate T-matrix light scattering, the diameter or radius of spherical particles are taken in the algorithm. Hence, the diameter is converted from the size of glistening, and all glistening particles are assumed to be sphere.

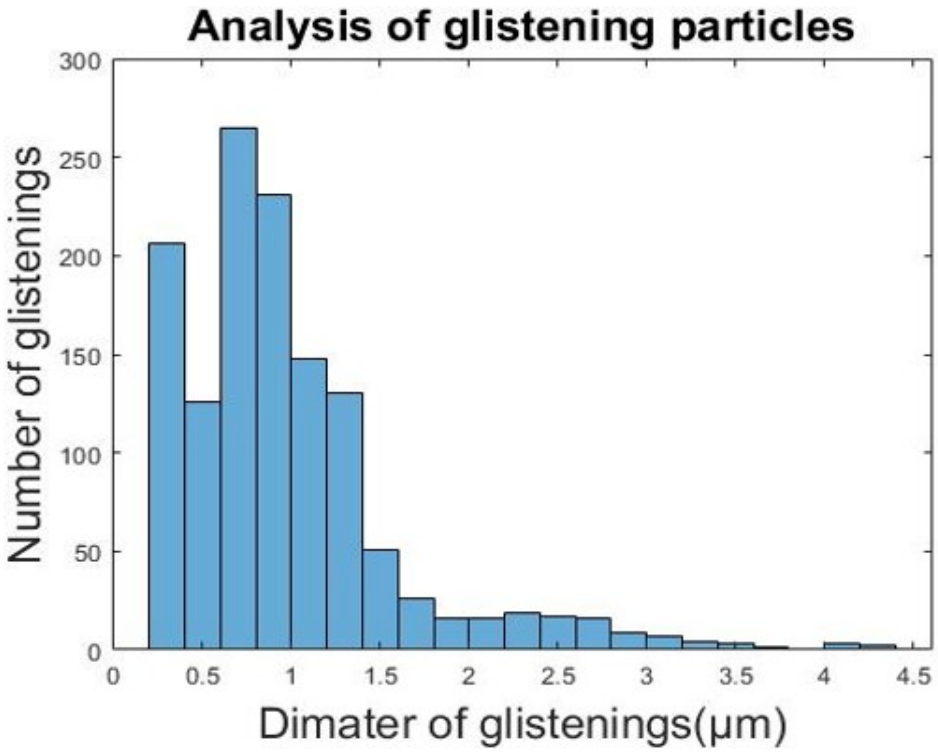

Figure 4.13: number and diameter of glistening from IOL image analysis

4.8.1 Diameter of glistening

The goal of using image analysis tools to IOL images is to achieve the specific data of lab-produced microvacuoles. After 48 hours of consequent heating in two different temperatures, the maximum size of glistenings can be seen around 4 µm and the minimum

size of glistenings can be found as 0.3 µm. Therefore, the standard deviation size of this experiment is 0.6 µm.

4.8.2 Number and density of glistening

According to previous studies, glistening grade depends on the time which takes IOL from water tub. In this research, grade 4 glistenings are achieved. By using bright field microscopic images, number of glistening are approximately 1300 particles are found. However, the distribution of glistenings was proportional to the pupil size and thus, the density of glistenings for different pupil sizes was measured at (3mm, 4mm, 5mm) Phillip.et. al (2016)[18] which is described as Figure.4.14. In all cases Phillip.et.al (2016)[18], the measured distribution appeared less than the predicted uniform values indicating that in intraocular lenses the glistenings distribution is not uniform among the lens but tends to show more glistenings in the center.

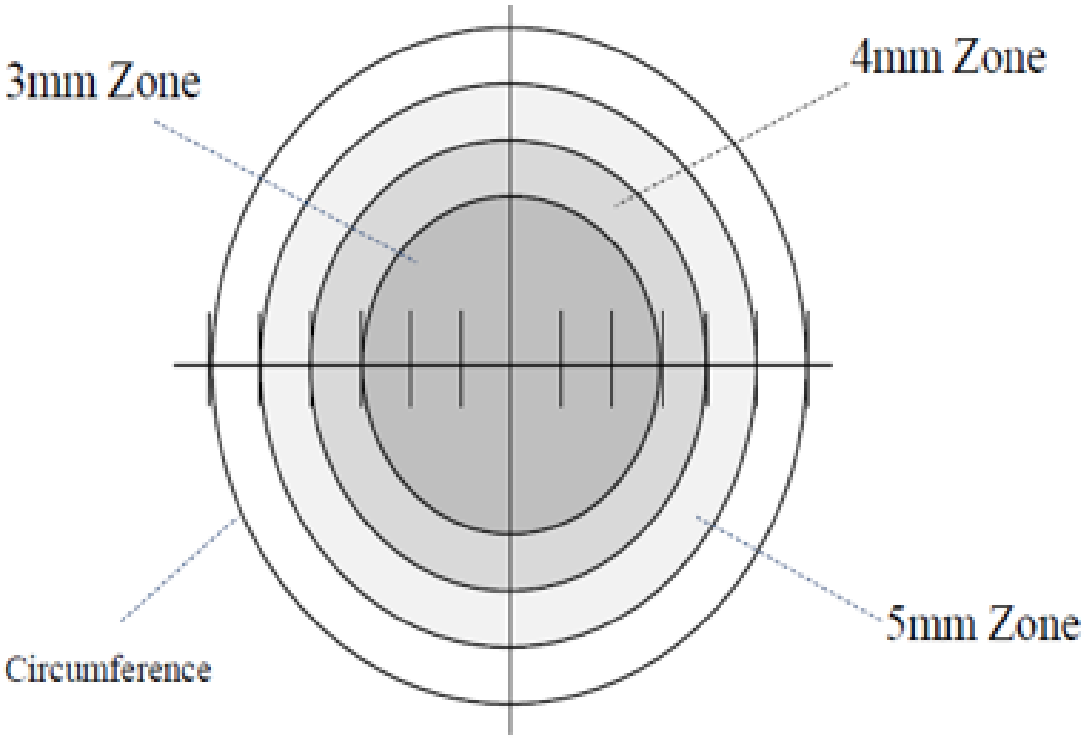

Figure 4.14: glistenings are defined by zone

4.9 Accuracy of Glistenings

Accuracy(%) measures that the proposed segmentation process can correctly identifies or excludes glistening in IOL images. To evaluate the accuracy of glistening detection from IOL images, five ground truth images are selected and defined manually defined. In this research, there are 25 images for one original image of IOL but the central part of the IOL is more important for light scatter calculation. Therefore, the central 5 rows of divided images are selected which are given names as Image1, Image2, Image3, Image4, and Image5. The segmentation evaluation algorithm is programmed with Matlab[54] which

is from the research of Thanh.et.al(2019)[55][56][57].However, the accuracy is defined by the following equation(Eqn.4.8) in which the correct result divided by the total number of segmented glistenings.

$$Accuracy = \frac{TP + TN}{TP + TN + FN + FP} \tag{4.8}$$

where TP, FP, TN, FN are defined as true positive, false positive, true negative, and false negative, respectively. However, the segmented glistening from IOL images are classified as four types.

- True Positive (TP): a number of pixel classified correctly as glistenings
- False Positive (FP): a number of pixel classified incorrectly as glistenings
- True Negative (TN): a number of pixel classified correctly as not glistenings
- False Negative (FN): a number of pixel classified incorrectly as not glistenings

From the Eqn 4.8, the accuracy is resulted as 90.58% for Image1 which has many small glistenings, 96.12% for Image2, 96.20% for Image3, 96.28% for Image4, and 94.07% Image5. There, the original microscopic images, detected glistenings in microscopic images and manual-defined ground truth are compared in the following Table 4.1. Nevertheless, the final result show that our method has the good performance with the average accuracy of 95%.

Table 4.1: Comparison of original, glistening detection algorithm and ground truth images

Image Name	Original Image	Detected Glistening	Ground Truth
Image1	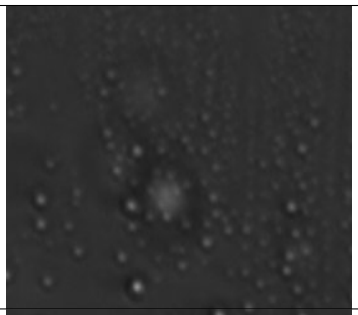	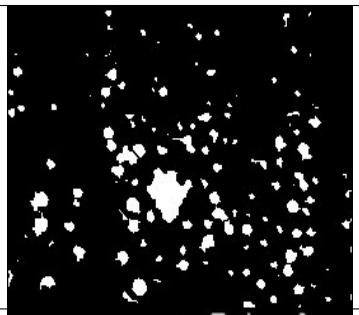	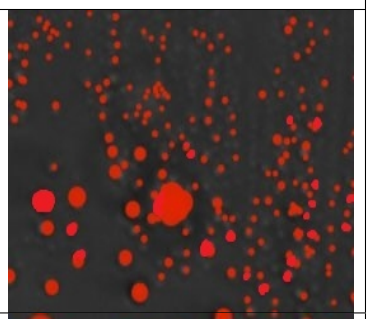
Image2			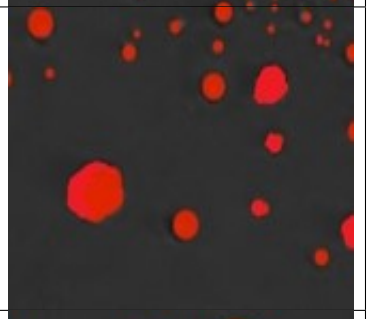
Image3		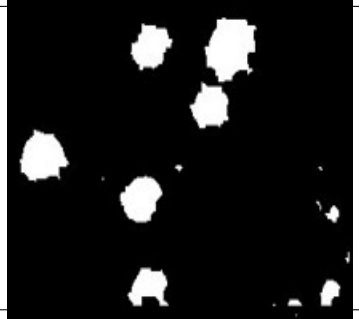	
Image4			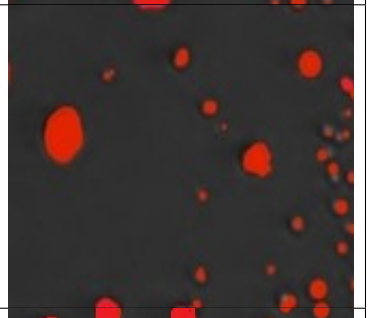
Image5	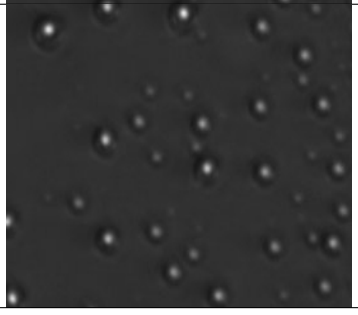	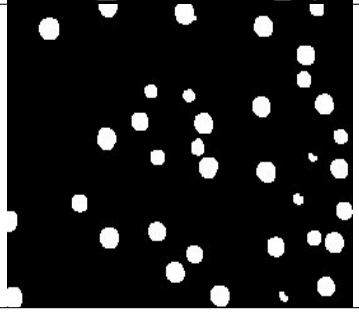	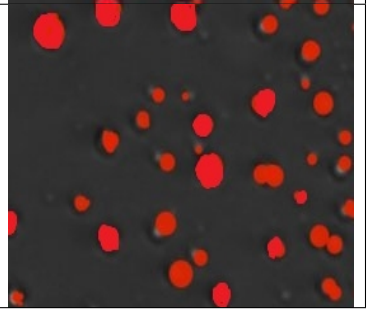

Chapter 5

Light Scatter Measurement

The impact of glistening in IOL causes light scattering which depends on the refractive index between the vacuoles and the lens material, as well as the size, density, and shape of the glistenings. Therefore, these important characteristics are obtained from image analysis of microscopic images of IOL and parameterized as input for light scattering calculation. Therefore, lens are prepared for this experiment by vitro method and discussed details in the scattering parameter section. Then, T-Matrix method is applied to calculate the light scattering but multiple light scattering is also considered. Next, CELES simulation tool[58] is used to visualize how light is scattering inside the lens.

5.1 Application of T-Matrix approach to light scatter calculation

Light is an electromagnetic wave that is discovered by Maxwell. Therefore, light scattering in this research is assumed as electromagnetic scattering which can be explained by the electric field(E) and magnetic field(H). In addition, light scattering in IOL was calculated by using T-Matrix method which is based on the expansion of incident, and the scattered field into a series of spherical vector wave functions [59]. Total electric field(E) is written as a sum of incident(E_{in}) and scattered fields(E_s).

$$\overrightarrow{E} = \overrightarrow{E_{in}} + \overrightarrow{E_s} \tag{5.1}$$

In fact, T-matrix is a particle response matrix that transforms the incident field expansion coefficients to the scattered field coefficients. Moreover, particle shape, size, refractive index, and the orientation of the particle are correlated to T-matrix. Therefore, the scattered field can be calculated for any incident field and any direction when T-matrix is known for a particle. To calculate for one sphere, the total electric field is the sum of an incident field and the scattered field. For multiple particles, the incoming field for each i^{th} particle is the sum of the initial excitation and the scattered field of all other N spheres:

$$\mathrm{E}_{in}^{i}(r) = \mathrm{E}_{i}(r) + \sum_{i' \neq i}^{N} \mathrm{E}_{s}^{i'}(r) \tag{5.2}$$

Since T-matrix approach is from the electromagnetic framework, the interaction between an illumination wave and scattering particles relies on the expansion of the incident wave

and of the scattered wave in terms of vector spherical wave functions (SVWFs) [60] in which RgM, RgN means the regular wave functions and M, N refers to the singular wave functions.

$$\mathrm{E}_i(r) = \sum_{n=1}^{\infty} \sum_{m=-n}^{n} [a_{mn} RgM_{mn}(kr) + b_{mn} RgN_{mn}(kr)] \tag{5.3}$$

$$\mathrm{E}_s(r) = \sum_{n=1}^{\infty} \sum_{m=-n}^{n} [p_{mn} M_{mn}(kr) + q_{mn} N_{mn}(kr)] \tag{5.4}$$

where k (wave number) $=2\pi/\lambda$, λ is the wavelength, r means the position vector and degree n and order m. According to Maxwell's equations, the scattered field coefficients p_{mn} and q_{mn} can be calculated from the incident field coefficients a_{mn} and b_{mn} by using a transition matrix.

$$\mathrm{p}_{mn} = \sum_{n'=1}^{\infty} \sum_{m'=-n'}^{n'} [T^{11}_{mm'nn'} a_{m'n'} + T^{12}_{mm'nn'} b_{m'n'}] \tag{5.5}$$

$$\mathrm{q}_{mn} = \sum_{n'=1}^{\infty} \sum_{m'=-n'}^{n'} [T^{21}_{mm'nn'} a_{m'n'} + T^{22}_{mm'nn'} b_{m'n'}] \tag{5.6}$$

Equation (6) can be written in a compact form as:

$$\begin{bmatrix} p \\ q \end{bmatrix} = T \begin{bmatrix} a \\ b \end{bmatrix} = \begin{bmatrix} \mathrm{T}_{11} & \mathrm{T}_{12} \\ \mathrm{T}_{21} & \mathrm{T}_{22} \end{bmatrix} \begin{bmatrix} a \\ b \end{bmatrix} \tag{5.7}$$

However, T-matrix takes account of mn indices, and thus a new variable l_{max} is defined as n(n+1) +m to know the maximum level of the matrix. Therefore, equation 6 can be written in details according to the levels of matrix (l_{max}).

$$\begin{bmatrix} p \\ q \\ \cdots \\ \cdots \\ \mathrm{p}_{lmax} \\ \mathrm{p}_{lmax} \end{bmatrix} = \begin{bmatrix} \mathrm{T}^{11}_{11} & \mathrm{T}^{12}_{11} & \cdots & \cdots & \mathrm{T}^{11}_{1,lmax} & \mathrm{T}^{12}_{1,lmax} \\ \mathrm{T}^{21}_{11} & \mathrm{T}^{22}_{11} & \cdots & \cdots & \mathrm{T}^{21}_{1,lmax} & \mathrm{T}^{22}_{1,lmax} \\ \cdots & \cdots & \cdots & \cdots & \cdots & \cdots \\ \cdots & \cdots & \cdots & \cdots & \cdots & \cdots \\ \mathrm{T}^{11}_{lmax,1} & \mathrm{T}^{12}_{lamx,1} & \cdots & \cdots & \mathrm{T}^{11}_{lmax,lmax} & \mathrm{T}^{12}_{lmax,lmax} \\ \mathrm{T}^{21}_{lmax,1} & \mathrm{T}^{22}_{lmax,1} & \cdots & \cdots & \mathrm{T}^{21}_{lmax,lmax} & \mathrm{T}^{22}_{lmax,lmax} \end{bmatrix} \begin{bmatrix} \mathrm{a}_1 \\ \mathrm{b}_1 \\ \cdots \\ \cdots \\ \mathrm{a}_{lmax} \\ \mathrm{b}_{lmax} \end{bmatrix} \tag{5.8}$$

However, $p = T \cdot a$ is used as a short description for next equations from Eqn 5.7 and 5.8 where $p = [p_{mn}, q_{mn}]$ and $a = [a_{mn}, b_{mn}]$. However, the purpose of using T-matrix is that allows a pair of spherical particles can be calculated as a single scatterer [61]. Yet, the multiple scattering takes account of the incoming field coefficients with the initial field and sum of scattering field coefficients from all particles. The sphere centered T^{ji} matrix is converted to the cluster-center T-matrix based on a single origin of the cluster as Figure 5.1.

$$\mathrm{p}^j = \mathrm{T}^j(\mathrm{a}^i + \sum_{i \neq j} \mathrm{A}^{ji} \mathrm{p}^i) \tag{5.9}$$

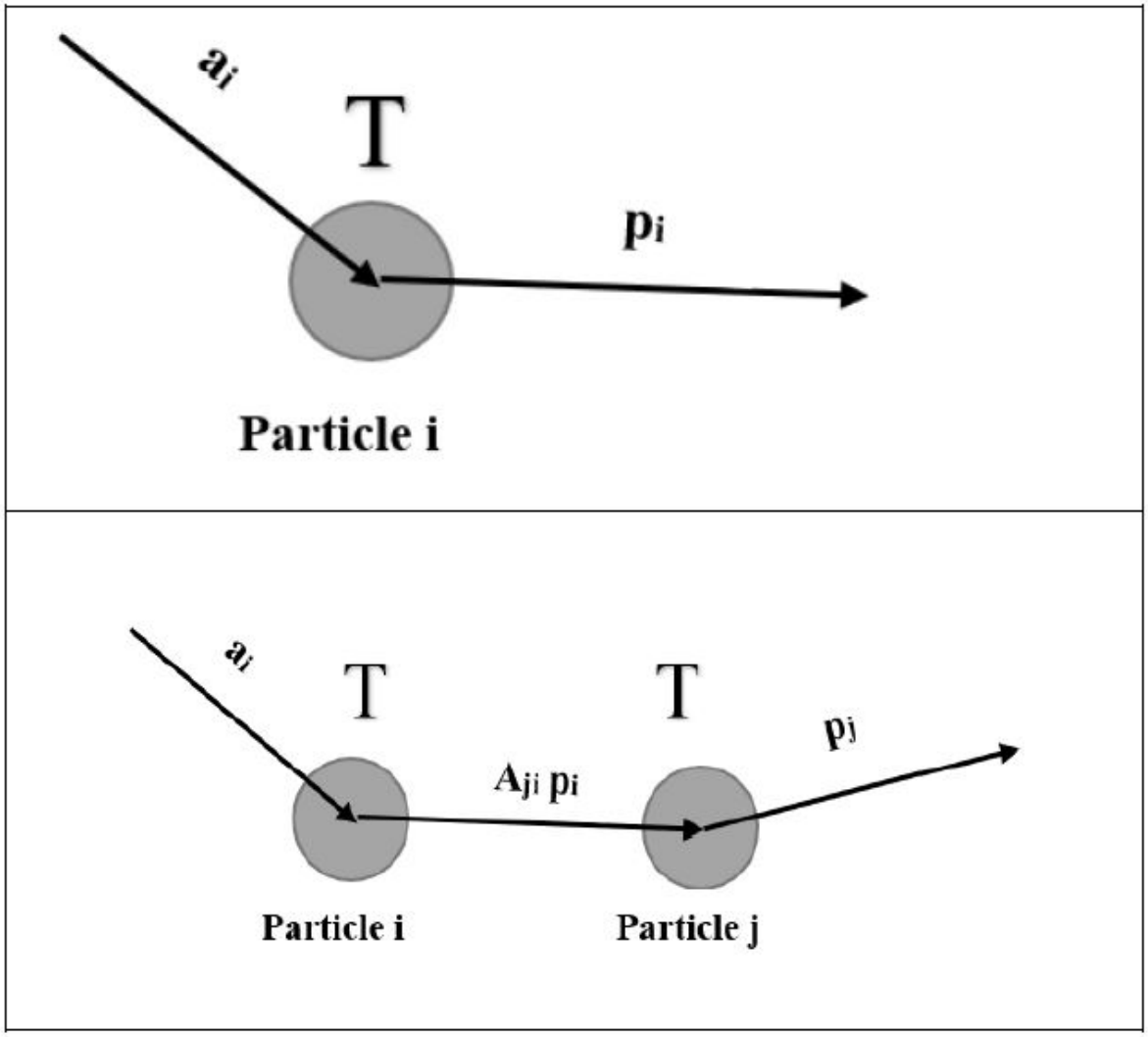

Figure 5.1: Block Diagram of Transition matrix in one particle and between two particles in which scattering field coefficients are calculated from incident field coefficients

The above equation is scattered field coefficient for sphere j can be calculated through the transition matrix of particle j, incident field coefficient of sphere i, and A^{ji} matrices. A^{ji} matrices are the electromagnetic interaction between two particles i and j, moreover, it is also related to the distance and orientation between these two particles. Therefore, transition matrix transforms the expansion coefficient of the incident field into the expansion of an individual scattered field.

$$\mathrm{p}^j = \sum_i \mathrm{T}^{ji}\mathrm{p}^i \tag{5.10}$$

Finally, multiple scattering problem is achieved as a single expansion of the particles that can be achieved from the scattered field expansions of the individual spheres where a and p are the incident and scattered field coefficients, B is also the matrices of the

electromagnetic interaction between two particles which is similar to A matrix.

$$p = \sum_{j} \mathrm{p}^{j} = \sum_{j,i} \mathrm{B}^{j}\mathrm{T}^{ji}\mathrm{a}^{i} = \sum_{j,i} \mathrm{B}^{j}\mathrm{T}^{ji}\mathrm{B}^{i}a = Ta \tag{5.11}$$

5.2 Light Transmission by Power Flux

Power Flux of the light is defined as the direction by the polar angle β and the azimuth angle α with polarization j by using this equation.

$$\mathrm{P} = \frac{2\pi^2}{\omega \mathrm{k} \mu_0} \sum_{j=1}^{2} \int d\alpha \int d\beta \sin\beta |g_j(\alpha, \beta)|^2 \tag{5.12}$$

However, it can also be expressed as this form:

$$\mathrm{P} = \sum_{j=1}^{2} \int d\alpha \int d\beta \sin\beta I_j(\alpha, \beta) \tag{5.13}$$

I is the radiant intensity by polar angle α and β.

$$I_j(\alpha, \beta) = \frac{2\pi^2}{\omega \mathrm{k} \mu_0} |g_j(\alpha, \beta)|^2 \tag{5.14}$$

However, radiant intensity of the scattered field from Eqn.5.14 can be calculated by transformation from the spherical wave expansion to a plane wave expansion. In this equation, Intensity value, I is transformed for each of the spheres and finally, added up the contribution of all spheres,

$$g_j(\alpha, \beta) = E_0 \frac{k^2\omega^2}{4\pi} \cos\beta \exp\left[\frac{-\omega^2}{4} k^2 \sin^2\beta\beta\right] x(\delta_{j1}\cos\alpha\delta_{j2}\sin\alpha) e^{-ikr_G} \tag{5.15}$$

where g means Gaussian beam.

Since the different grades of glistenings describe that number of multiple vacuoles can also be located closely in IOL. Therefore, light scattering for one particle is not sufficient and multiple light scattering for glistening clusters is also required. For this purpose, CELES, Matlab toolbox which runs on graphics processing units (GPUs) is used to simulate and compute multiple-sphere T-Matrix method. As the output of this research, power reflectivity and transitivity values (power transmission and loss) are computed to identify the lens transmission of IOL. In particular, the flow chart of research is described in the following Figure.5.2.

5.3 Result of CELES Simulation

The resulting form CELES simulation software is explained in this section. Figure 5.2 can also describe how light scattering is calculated. Firstly, we simulated to visualize how glistening particles located in IOL and how the total electric field after incident wave is scattered through the particles since glistening is densely closed and multiple scattering

occurred in this condition. Next, light transmission and loss through IOL due to whitening and glistenings are calculated.

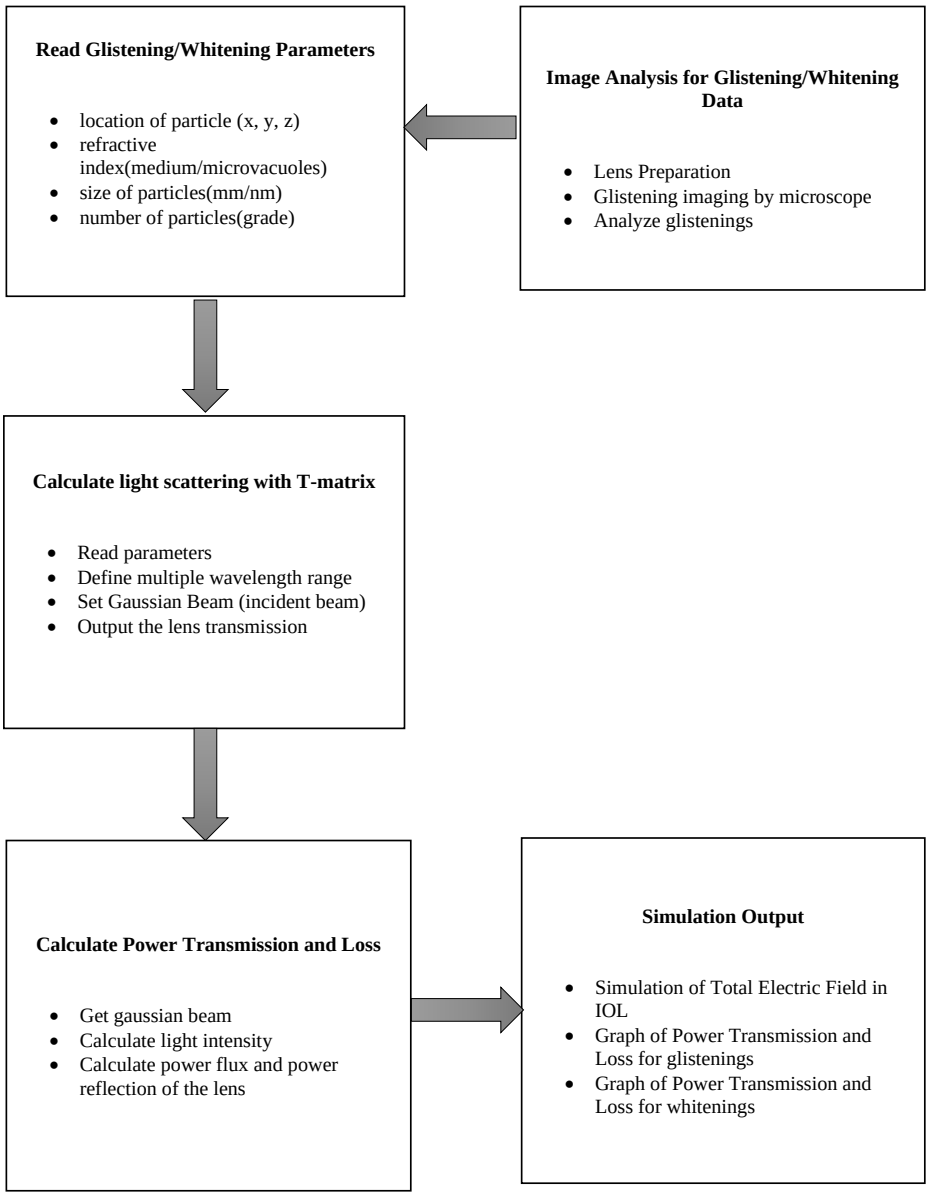

Figure 5.2: Simulation of light scattering by CELES

5.3.1 Simulation of Total Electric Field

Figure.5.3,5.4,5.5 and 5.6 show the position of spherical glistenings in IOL with coordinate system and how the total electric field after incident wave is scattered through the particles since glistening is densely closed and multiple scattering occurred in this condition. In fact, the right figure from Figure.5.3 to 5.6 is plotting the result from Equation 5.1 as the function: $E(r) = E_{in}(r) + E_s(r)$. Although different grades of glistenings are changed

in this simulation, three different IOL sizes are randomly selected. Near-field intensity is not affected while glistenings are freely located. In different circumstances, the densely packed glistening (grade 3 and grade 4) from the second pictures Figure. 5.5 and 5.6 show that electric field intensity is stronger because of the coupling effect from multiple lights scattering through these particles.

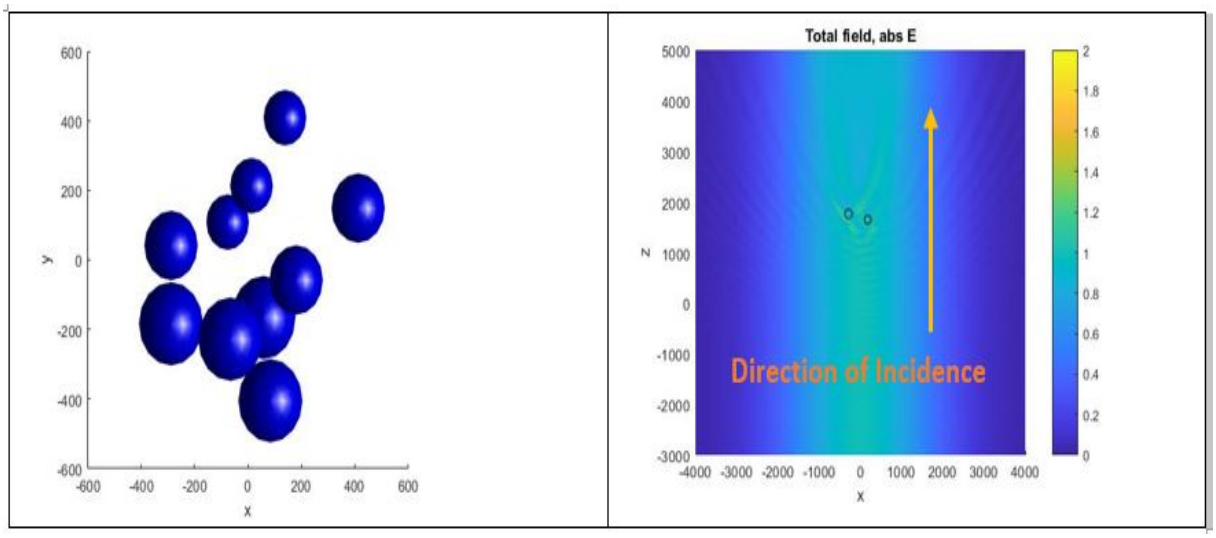

Figure 5.3: Position of Grade 1 glistenings and total electric field after light scattering

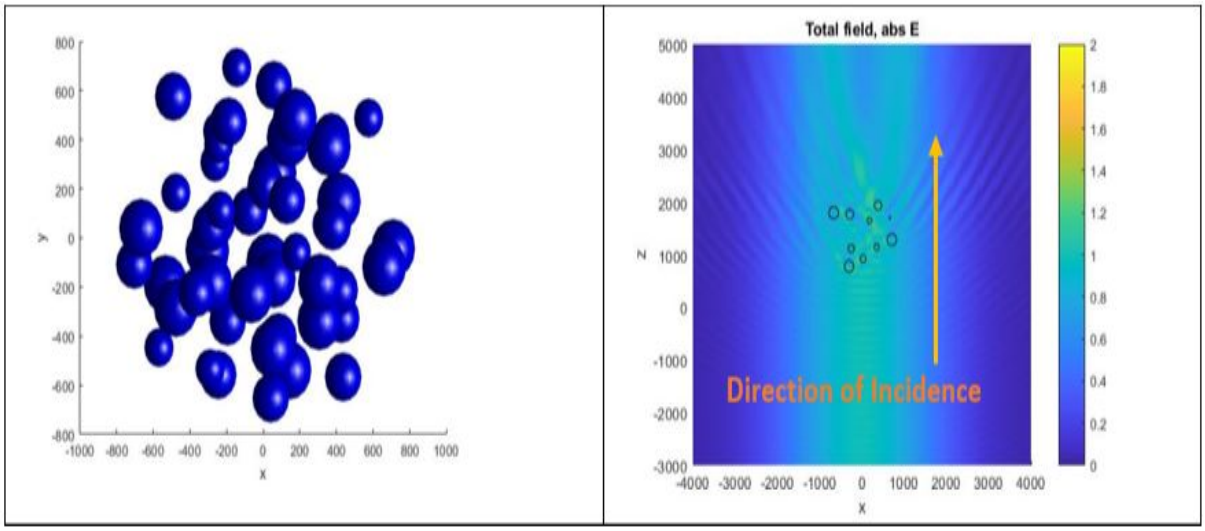

Figure 5.4: Position of Grade 2 glistenings and total electric field after light scattering

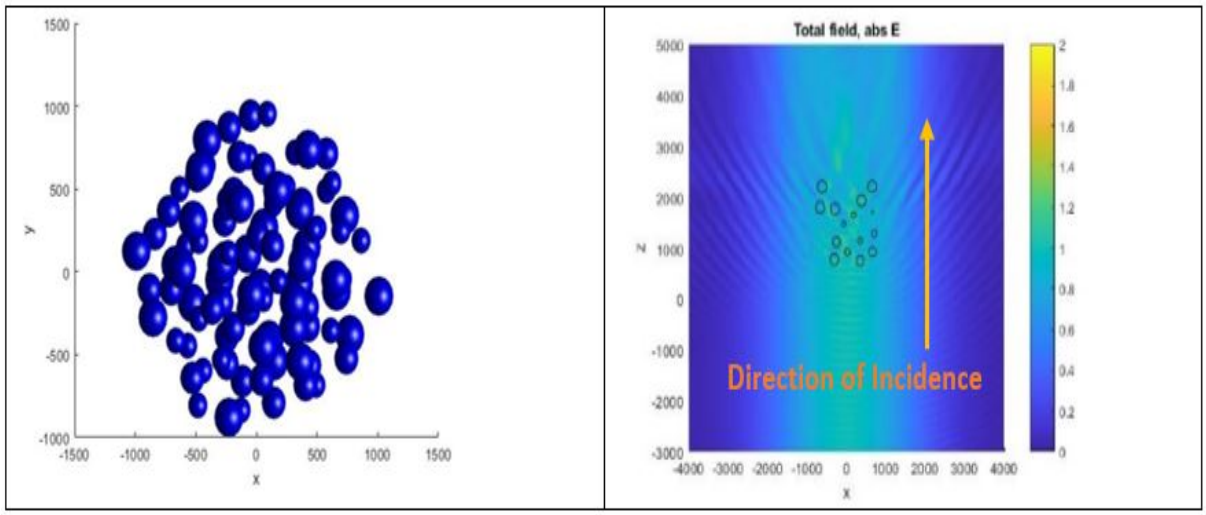

Figure 5.5: Position of Grade 3 glistenings and total electric field after light scattering

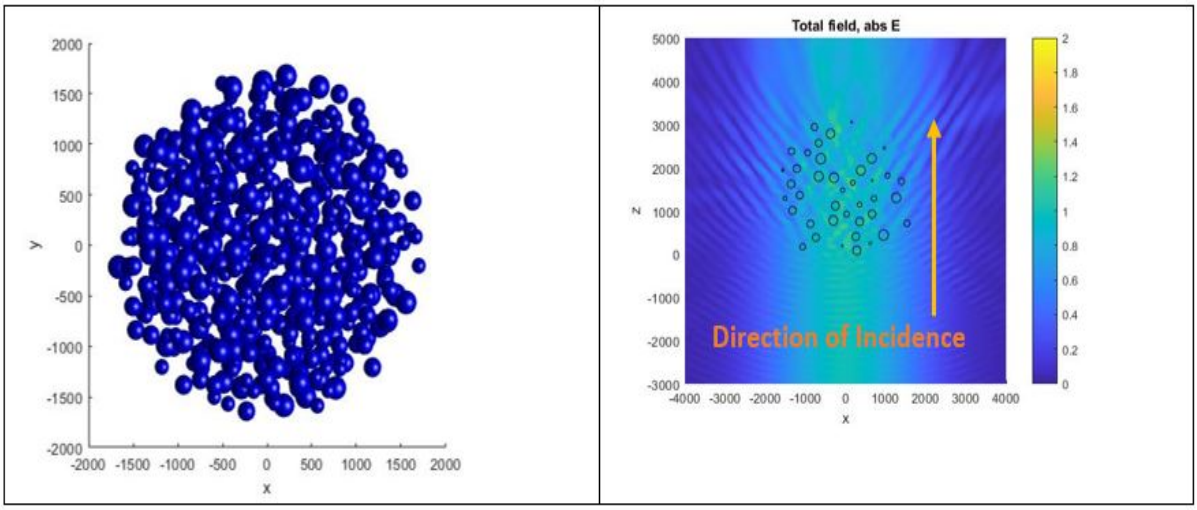

Figure 5.6: Position of Grade 4 glistenings and total electric field after light scattering

5.3.2 Power Transmission and Loss

Power transmission and loss of IOL are calculated using Eqn. (5.12) in which the Gaussian beam is used as an incident beam. Glistening and whitening are defined and set the size of their values. All the data for the size and grading values are reviewed from the image analysis of microscopic IOL. To determine the changes of size effects on the light transmission through IOL, different sizes from the result of glistening counting are selected. Since the difference between glistenings and whitenings is microparticle size and nanoparticle size. Therefore, the glistening size is set micrometer while the whitening size is set to nanometer. The first two picture is power transmission and loss of glistening where the different grade of glistenings are presented with visible wavelength range (between 370nm and 780nm). Although 4 different grades are compared for both microvacuoles and nanovacuoles, the significant value of transmission and loss can be found in this

grade. Therefore, we discuss only for the transmission and loss of grade 4 in the next section. However, the correlation between different size and visible wavelength is shown as the result of simulation with CELES in the following Figures 5.7 and 5.8.

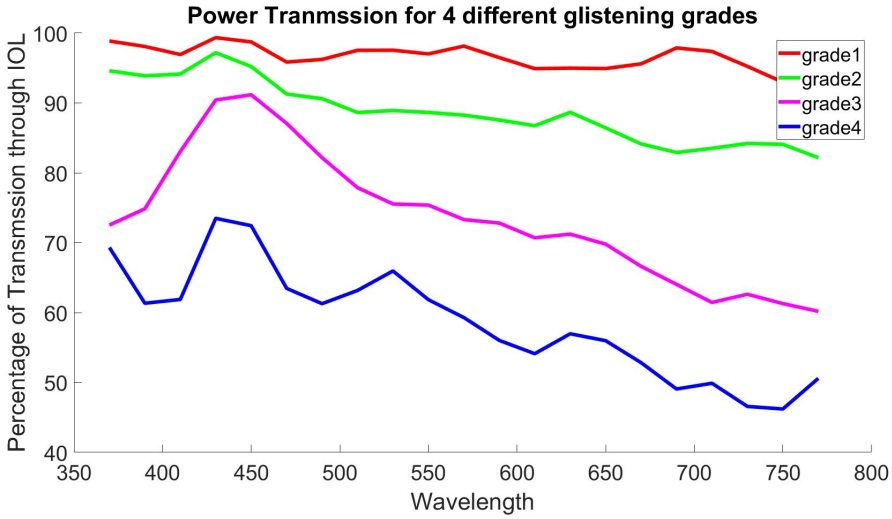

Figure 5.7: Power Transmission of IOL for glistening

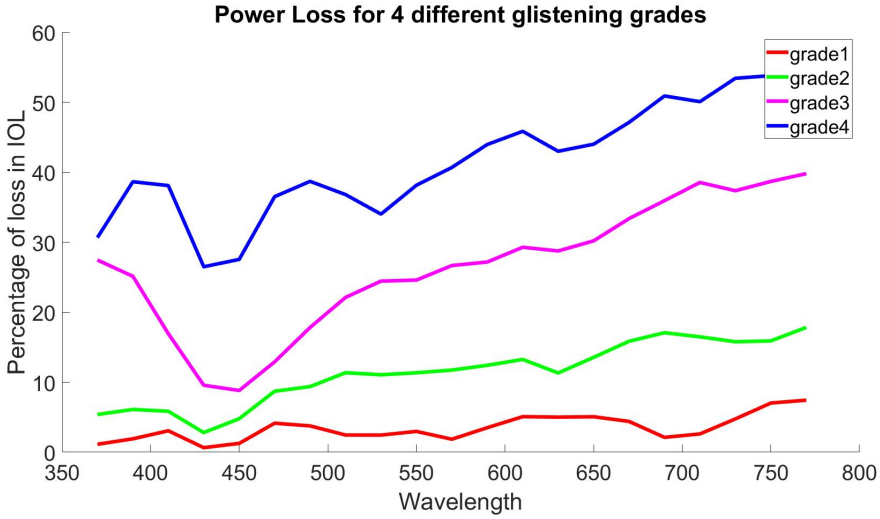

Figure 5.8: Power Loss of IOL for glistening

As seen in Figure 5.9 and 5.10, Power transmission and loss for glistening are related to the visible wavelength. Overall, the power transmission of IOL for all glistening grades declined over the wavelength, whereas transmission value reaches the peak at wavelength() between 400nm and 450nm. Afterward, the trends go down steadily until 780 nm. On the other hand, power loss values are increasing but the lowest loss value is also found at the wavelength range between 400nm and 450nm. Except from this point, power transmission is decreased while loss values are increased over the wavelength. However, grade 4 glistenings have the highest loss value 49% and lowest transmission with 51% within a visible wavelength range. To conclude, we can estimate that the power transmission value will fall when the glistening number is increased.

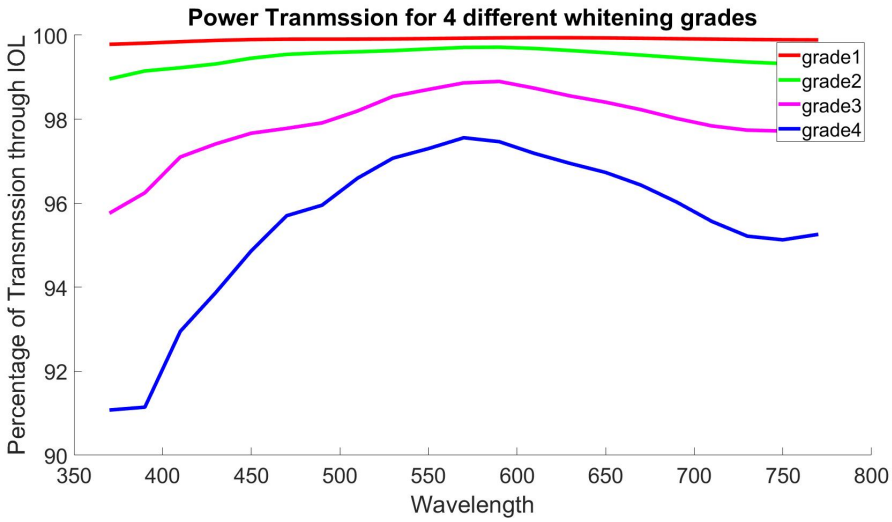

Figure 5.9: Power Transmission of IOL for whitening

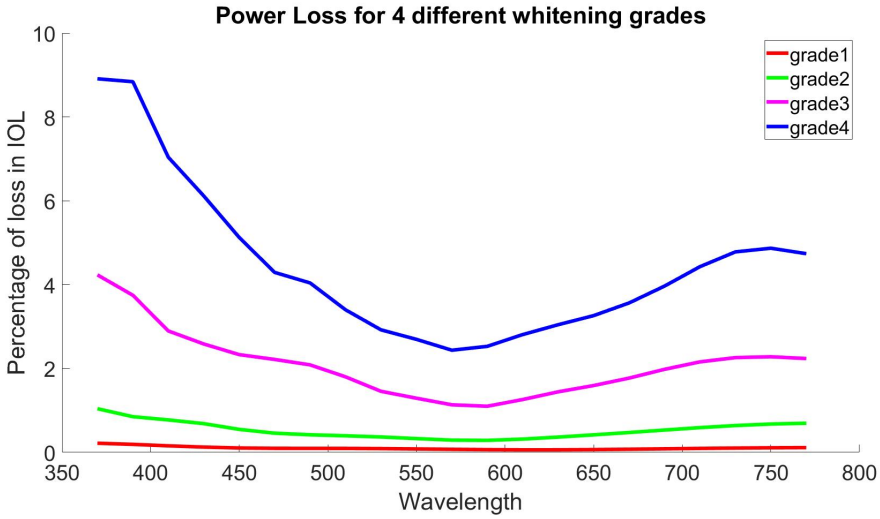

Figure 5.10: Power Loss of IOL for whitening

Chapter 6

Visibility Evaluation of Intraocular Lens

Visibility functions of IOL with glistenings are evaluated through glare and contrast sensitivity from the optical model. Glistenings give arise light scattering in IOL and as a result of intraocular light scatter called straylight in retina, disability glare. The quality of human vision depends on the image in the retina and disability glare can cause the loss of retinal image contrast. Since the incoming light source is scattered within human eyes and appear "veil" of luminance to the object, disability glare is also called veiling luminance. Moreover, glare can also be caused by imperfections in the optical system due to age, iris pigmentation, cataracts, and straylight in the cornea. However, glare can affect human activities for both daytime and night time. Consequently, disability glare comprises visual complaints such as hazy or blurry vision.

Veiling luminance which is the effect of glare in vision is formulated in terms of an equivalent veiling luminance which is shown in Eqn.6.1. Holladay et.al (1927) [62] introduced this equation from investigations of correlation between glare source luminance and its distance from the object. In this research, veiling luminance is assessed from the illuminance at the eye of the observer due to the glare sources and the angular separation of the glare source.

$$\mathrm{L}_v = \frac{kE}{\theta^n} \tag{6.1}$$

Although there are many lighting application standards to define the straylight parameter (k), Hollday.et al (1927) [62] describe the value of k to be 10 and scatter index(n) is taken to be 2. Moreover, E is the illuminance of the light entering the human eyes from the glare source and θ the angle in object space. From this equation, the visual veiling luminance of a glare which is the result of intraocular light scatter can be evaluated. However, illumination from the light source is important to quantify the glare and this research computed the illumination of light to the surface of the human retina from light scattering theory called T-matrix.

6.1 Retinal Illuminance(E) from the glare source

Light scatter contribution in IOL is analyzed from different characteristics of glistenings and quantified by using T-matrix in the previous chapters. As a result, light transmission

through IOL is computed as radiant power from electromagnetic scattering and thus, the power flux conversion from the radiometric unit to the photometric unit for human eyes is necessary. In fact, radiant flux measures all electromagnetic radiation emitted (including infrared, ultraviolet, and visible), which is the total amount of objective light. The SI unit of radiant flux is the watt (W). However, luminous flux is the amount of light that the human eye senses where SI unit of luminous flux is lumen [63]. The objective of conversion from radiant flux to luminous flux is to evaluate retinal illuminance from the light source through glistening obstacles. Therefore, the first step is to take the radiant flux value which is transmitted through IOL based on the different wavelengths of the incoming light.

$$Luminous flux(P) = (Radiant flux) \times Km \times V(\lambda) \tag{6.2}$$

In the above equation, radiant flux value is from the result of light scattering calculation of T-matrix. Furthermore, the photopic spectral luminous efficiency curve V(λ), which gives the spectral response of the human eye to various wavelengths of light. The following table 6.1 is defined V(λ) according the CIE photopic spectral luminous efficiency function.

Table 6.1: Spectral Luminous Efficiency Functions [64]

wavelength(nm)	Luminous efficiency (V(λ))
370	0.00004
390	0.00012
410	0.00120
430	0.01160
450	0.03800
470	0.09100
490	0.20800
510	0.50300
530	0.86200
550	0.99500
570	0.95200
590	0.75700
610	0.50300
630	0.26500
650	0.10700
670	0.03200
690	0.00820
710	0.00210
730	0.00052
750	0.00012
770	0.00003

Moreover, Km value is set to 683 lm/W which has the maximum sensitivity for the

photopic vision which occurs at 555nm wavelength. However, the number of glistenings can affect the light scattering in IOL, and thus, different grades of the glistenings are also considered in retinal illumination. Since illuminance means luminous power per unit area, the next step is to find the area of the image on the retina. The following equation is used to calculate Retinal Illuminance(E) from the light source. However, this research is evaluated from Vitro approach which has not experimented on the human body. Therefore, the light source to calculate light scattering through IOL is set up with a monochromatic Gaussian beam.

$$E = \frac{P}{A} \tag{6.3}$$

From the above equation, P is the luminous power and A is the area of the source in the retina. To calculate the area of the source on the retina, the area equation $A = \pi d^2$ in which d is the spot diameter of Gaussian beam area. The following figure shows how light enters the IOL and focuses on the retina.

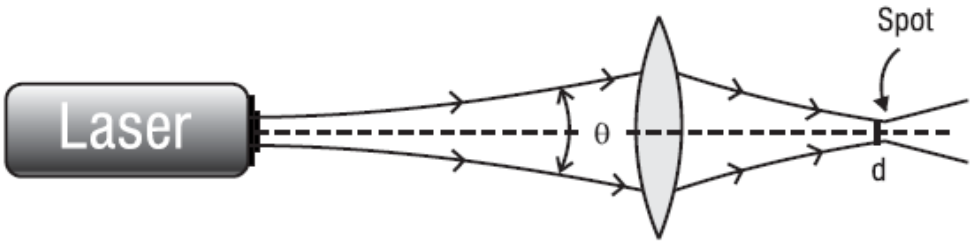

Figure 6.1: Light Transmission through IOL and focus on retina[65]

The above Figure 6.1 shows the beam divergence(θ) which is defined from the Gaussian beam. In Gaussian beam, beam divergence can be defined as follows:

$$\theta = \frac{\lambda}{\pi\omega_0} \tag{6.4}$$

where λ is the wavelength of incoming length and ω_0 is the waist of Gaussian beam which is defined as 4µm in light scatter calculation with T-matrix. Next, spot diameter d is computed as:

$$d = f\theta \tag{6.5}$$

The spot diameter on the retina depends on the focal length(f) and beam divergence(θ). The focal length of the human eyes is 17cm and thus f value is set in the above equation. Then, the area of the source in retinal is calculated by A= πd^2. As a result, retinal illumination from the glare source which is passed IOL with glistenings is acquired. According to Eqn.6.1, veiling luminance L_v is calculated from the retinal illuminance(E) which is emitted from the glare source. However, Eqn. 6.1. $L_v = [kE/\theta^n]$ is based on the visual angle(θ) which depends on the distance between the object and the observer. This research use three visual angle which are 15°, 20° and 30°. Therefore, veiling luminance values(L_v) are obtained from the retinal illuminance(E) and compare with the 3 different glistening grades in the following figures. Since grade 1 glistening has small number of glistenings, the effect of light transmission can be ignored.

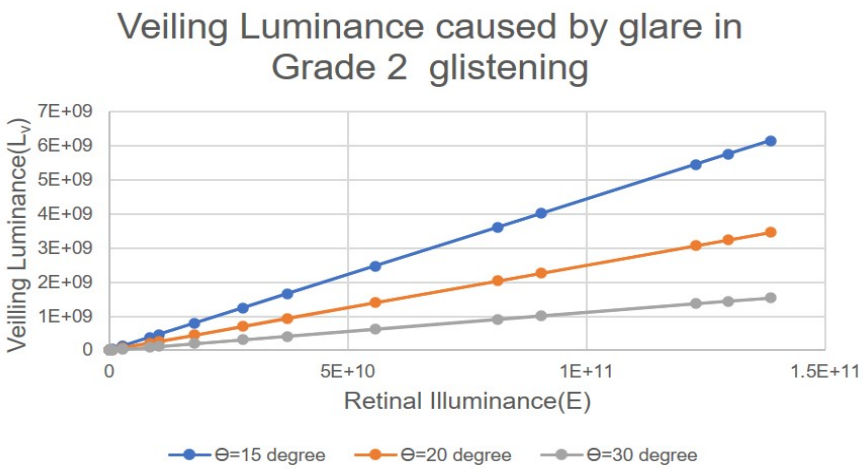

Figure 6.2: Varing of veiling luminance according to incident glare source for grade 2 glistening

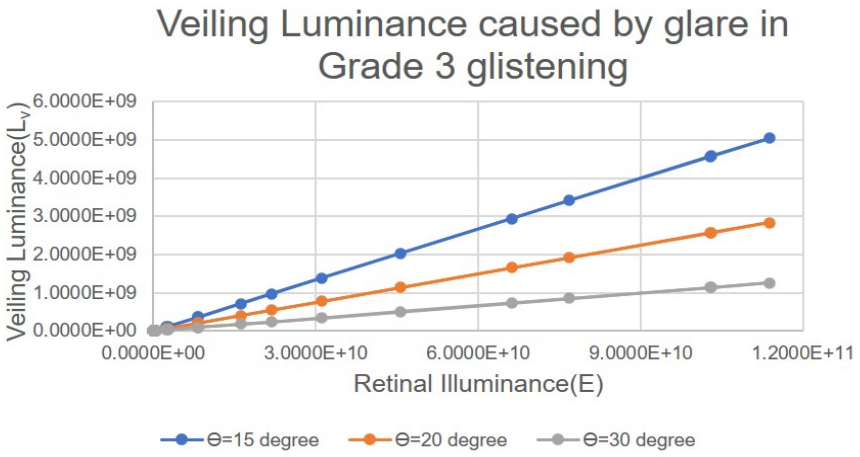

Figure 6.3: Varing of veiling luminance according to incident glare source for grade 3 glistening

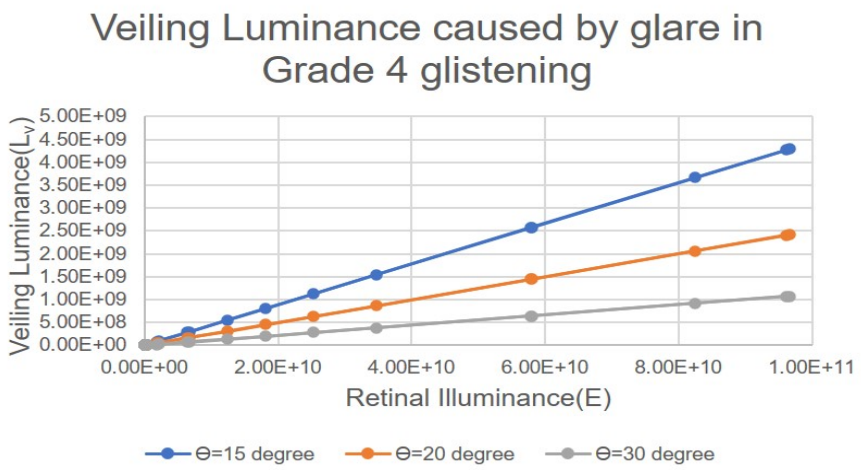

Figure 6.4: Varing of veiling luminance according to incident glare source for grade 4 glistening

From Figure 6.2,6.3 and 6.4, veiling luminance values are calculated for each of the glistening grades. However, these veiling luminance values(L_v) depend on the grade of the glistenings and thus, L_v is studied for each of the group. When the glistening numbers are increasing in each of the grades, the light reaching to retina(E) is decreasing. In grade 2, the highest retinal illuminance values are around 1.3E+11 cd at wavelength 550nm. However, the retinal illuminance values decreased to 1.1E+11 cd in grade 3 and 9.6E+10 cd in grade 4 respectively at wavelength 550nm by reason of veiling luminance. These illuminance values are directly calculated from Gaussian beam in the previous vitro experiment. Therefore, these values are normalized between 0 and 1 to compare the difference of glistening grades on veiling luminance. The following Figure 6.5 is the result of glare comparison for 3 different grades at two visual angles 15°and 30 °.

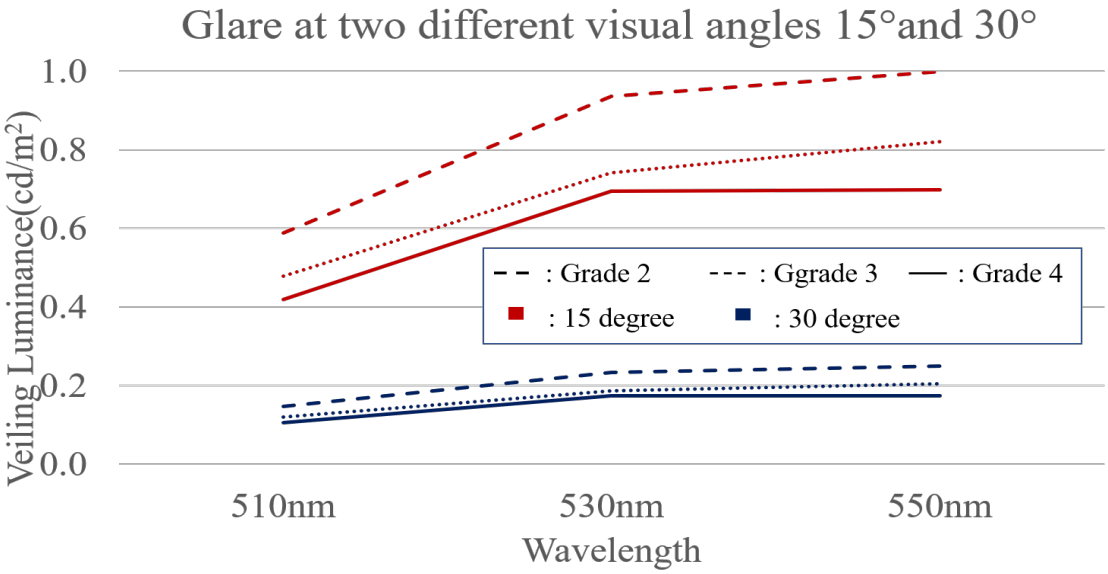

Figure 6.5: Disability Glare by Different Grade of Glistenings at visual angles 15° and 30°

6.2 Glare and contrast sensitivity

Since the glare and contrast sensitivity are correlated, the effect of glare is studied in this section as the reduction of contrast according to the following equations[16]. However, some of the scene is set up from Konrad et.al(2012)[66] are used in the evaluation of vision quality by the reduction of image contrast. Table 6.2 shows the luminance values of the scenes that can be seen at the night time driving in Poland. The location of billboard is about $1.5m$ to $13m$ above the ground from fields of view of the driver and size of billboard is around $30m^2$.

Table 6.2: Luminance from different scenes [66]

Luminance [cd/m^2]	Average Luminance(L_o)	Maximum Luminance (L_{max})	Minimum Luminance (L_{min})
Billboard's central point	1983	7953	377
Billboard's surroundings	9.3	108	0.9
Horizon of billboard	1.8	6.5	0.2
Road Surface	3.1	4.6	1.1

The luminance values of different scenes from table 6.1 are used to evaluate the reduction in contrast by the following equation.

$$C_a = \frac{L_0}{(L_0 - L_v)} \tag{6.6}$$

where C_a refers to contrast attenuation which is reduction of contrast by the glare, L_0 is average luminance and L_v is veiling luminance due to glare which is the effect of glistenings. From this equation, veiling luminance(L_v) is calculated from Eqn.6.1 that is based on the light transmitting to retina through IOL with glistenings. However, these luminance values are from Gaussian beam and thus, these values are higher than average luminance of all the scenes. For example, average luminance of billboard central point is $1983cd/m^2$ while the veiling luminance of the eye is around 6.15E+09cd/m^2 in grade 2 glistenings. Therefore, veiling luminance values are normalized to be the same range of luminance in the nighttime driving. Finally, reduction of contrast sensitivity values are shown in Figures 6.6, 6.7, 6.8, and 6.9 with 4 different grades to evaluate how much visual quality is degraded.

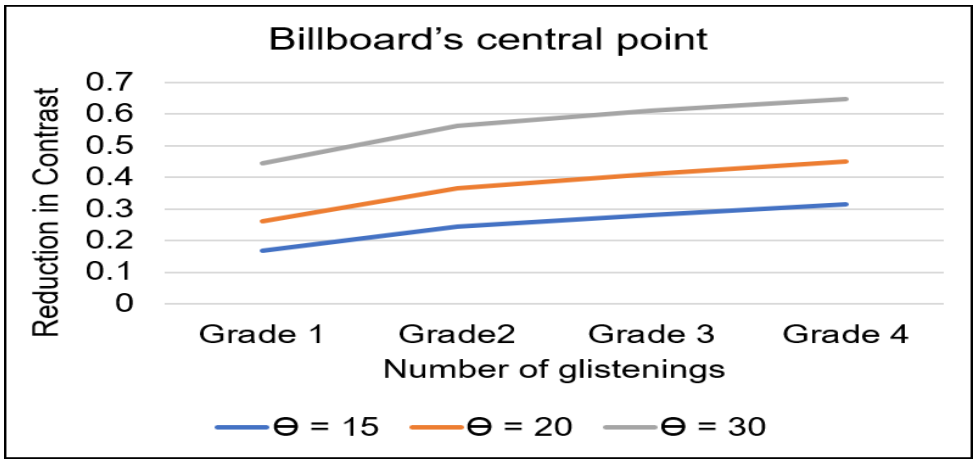

Figure 6.6: Reduction of Image Contrast by glare at Billboard's central point

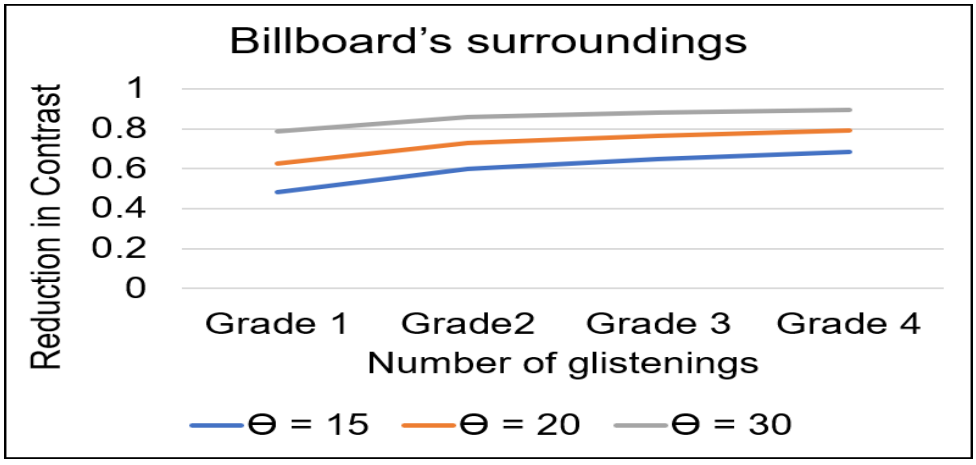

Figure 6.7: Reduction of Image Contrast by glare at Billboard's surroundings

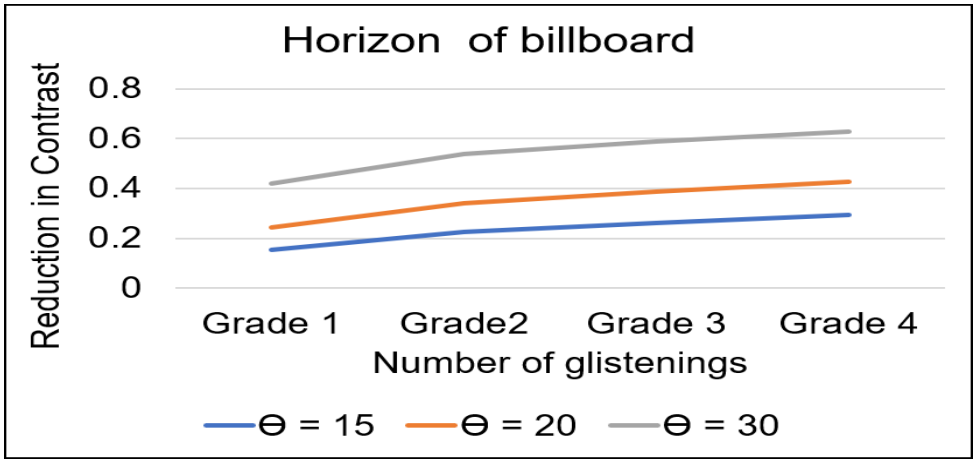

Figure 6.8: Reduction of Image Contrast by glare at Horizon of billboard

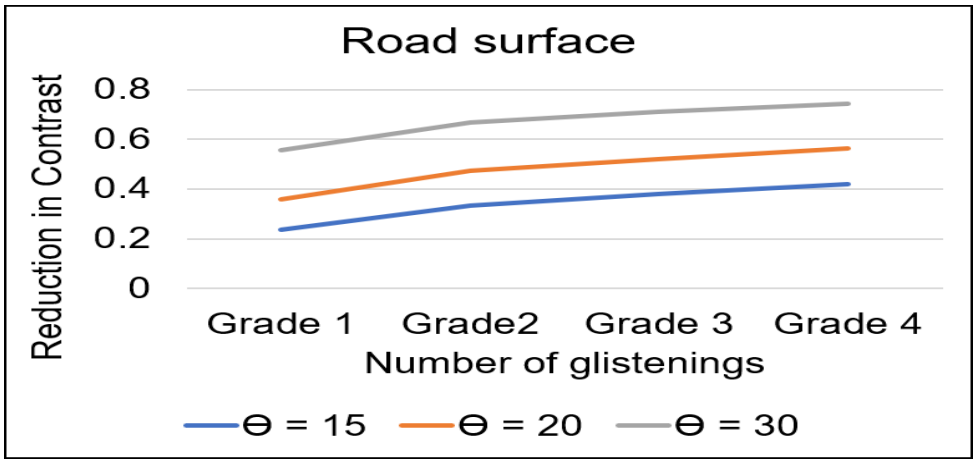

Figure 6.9: Reduction of Image Contrast by glare at Road Surface

Although the scenes are different in the above figures, all the contrast values are reduced as a result of glare in the presence of glistenings. In the first scene, the driver is looking at the billboard's central point while driving at the nighttime. Since glistenings are in the IOL of driver's eyes, disability glare is occurred and the contrast is reduced. However, the number of glistenings can be different and thus, the reduction of contrast values are also varied for each of the visual angles. The visual angle 30°affect largely since the loss of contrast around 60% as the highest rate. On the other hand, 15°also reduce the contrast but the reduction is around 30% as the largest loss. However, the other scenes also affect the vision quality by cause of glare and the loss is around 80% in billboard's surrounding and road surface. These loss values can affect the driver's safety at the glistening grade 4. Therefore, glare with glistening grade 4 can reduce the contrast of retinal image quality which will affect the daily activities.

Chapter 7

Conclusion and Future Work

The research is concluded in this chapter. The goal of this research is to achieve an optical model of glistenings with IOL in which visibility function is evaluated from different glistening characteristics, human activities, and light scatter conditions. For this purpose, the main processes are discussed in Figure 1.2 of Chapter 1. According to that block diagram, this research includes glistening generation, image analysis, light scatter measurement, and visibility evaluation. Before we discussed these steps, related works from previous literature are described in chapter 2. In this chapter, we categorized two main groups to identify the research goals from different methodologies due to the research structure.

Basically, we named clinical studies and mathematical studies from the research that is mentioned in chapter 2. From this work, we intended to understand the problems of glistenings, methodologies, and drawbacks of the previous research. In clinical studies, the light scattering problem is solved by using clinical devices such as C-Quant straylight meter and Scheimplfug camera. Moreover, vivo research also needs patients to participate while vitro research is not required. However, this kind of research is costly and time-consuming because experts of the clinics must support to use these devices. Moreover, the result can also not be accurate since the setting of human activities is not considered in these experiments. For example, glistening can affect the vision of humans but the result can be different according to the activities at that time. Driving at night and studying at the room are not the same conditions of lighting and thus, the function of rod and cone cells also differ. These conditions are not considered in both clinical and mathematical studies. Mathematical studies also based on theories of light scattering and simulate the result with commercial software to visualize the results. From these reviews, we studied that optical model can solve the real problem situations because it can offer convenience and cost advantages over the required information on reality. Moreover, complex problems in the future can be solved with ease by providing information and impact in changing conditions.

In this research, we generate glistenings in the laboratory as vitro studies because the quality of available images from patients is not enough to identify glistening characteristics. Therefore, glistening is created by changing two different temperatures and captured with an inverted microscope. In this point, the microscope type, resolution, and magnifier are very important to capture glistening in IOL. Since glistenings are micro-sized particles, it is difficult to see these vacuoles by human eyes or ordinary microscope and light must pass through the lens to see the glistenings. In an inverted microscope, the

inverted microscope is designed with the light source and the "condenser" lens above the specimen. The condenser lens concentrates the light. The "objective" and turret of the microscope is on the bottom. The objective focuses the light to produce a real image. Moreover, specific magnifiers can only give the focus images. From this step, glistening images are captured and collected for the next step.

In image analysis, the collected microscopic images are applied in image processing techniques, Then, glistening features are identified by using image segmentation. Although microscopic images provide the optimal resolutions, some of the noises and imperfections are still in the images. Hence, background subtraction is important as the first step. Despite threshold images that can give the edges of glistenings to count and measure the size, glistening particles are closely located and overlapping particles are divided by using watershed algorithm. Finally, the number of glistenings is counted and sizes are also measured from this step. The result of chapter 4 is to reveal the glistening characteristics which are important properties light scatter calculation in the next chapter.However, the position of glistening is one of the parameters to calculate the light scattering in IOL by using T-matrix method. In this research, the glistening images can be available only 2D due to limited resources. The reconstruction of 3D glistening images in IOL is the future study and then, we can calculate the glistening data from the IOL which is generated in our laboratory. However, we assumed glistening as spheres and homogeneous distributions, and thus, the positions of glistenings can be independent.In the future, three dimensions reconstructions can be replaced, and thus, glistenings data can be accurate and light scattering can also be quantified with the real data.

This research introduces the theory of light scattering and multiple light scattering problems with electromagnetic light scattering theory. From the lab-induced microvacuoles, glistenings numbers are the same as grade 4 in IOL and thus, it is critical for light scatter problem. Since many glistenings are found in IOL and some of them are closely located, near filed electric field will be affected. Therefore, multiple light scattering problem is calculated from these IOL lenses. To visualize how glistenings are in IOL, CELES simulation tool is used. Moreover, total light transmission from IOL are also computed. Finally, power transmission through IOL to the retina is investigated from this research. However, there are various methods to measure light scatter that can be divided into three categories: the optical in Vitro, the optical in Vivo, and the psychophysical. Vitro means the experiment in the laboratory and thus, glistenings are not in human IOL. Therefore, it can measure forward scattered light directly by using light sensors. Vivo can be defined as the experiment in the human body and thus, light scatter is measured in human IOL. Nonetheless, human eyes are the closed system and thus, it is difficult to measure forward light to the retina. Hence, the measurement of optical in Vivo scatter can proceed indirectly from light reflected out of the eye. Finally, psychophysical methods in which light scatter is quantified by estimating the amount of diffused light creating veiling glare which reduces the contrast of the retinal image. In this research, we approached from the psychophysical method in Vitro study, and thus, light scatter of IOL can be evaluated by using the commercial instrument (C-Quant) which measures the straylight of IOL with glistenings or without glistenings. However, we have limited time and resources for this research, this is the future work to evaluate the light scattering calculation from our research.

Moreover, the visibility of IOL is evaluated from the point of glare and contrast sensitivity. Since this research is proceeded by vitro approach and thus, laser light is used

to create a glare source. This research is intended to approach visibility evaluation in Vitro study and thus, light conditions for Vivo research can be extended in the future. However, the previous research considers the glistening numbers only in the grading of glistenings in IOL. This research considers not only glistening numbers but also the optical phenomenon to define glistening grading. Moreover, we proposed an optical model in which glistening characteristics are defined as scatter parameters, calculates multiple light scattering, and evaluates the visibility function based on light condition(day/night) and human activities such as driving, studying and exercising.

Publications

[1] K. T. M. Han, K. Kotani, P. Siritanawan, W. Kongprawechnon and C. Sinthanayothin: "Analysis of power transmission through IOL with glistenings and whitenings by T-Matrix," Journal of Quantitative Spectroscopy and Radiative Transfer, Volume 253,2020,107083,ISSN 0022-4073,https://doi.org/10.1016/j.jqsrt.2020.107083.

[2] K. T. M. Han, K. Kotani, P. Siritanawan, W. Kongprawechnon and C. Sinthanayothin: "Simulation of Multiple Light Scattering in Intraocular lens with glistenings by T-Matrix," International Conference on Advanced Information Technologies (ICAIT), Yangon, Myanmar, 2019, pp. 126-131, doi: 10.1109/AITC.2019.8920838.

[3] K. T. M. Han, B. Uyyanonvara, K. Kotani and P. Siritanawan,C. Hull: "Deep Learning forGlistening Quantificationin Intraocular Lens," Proceedings of the World Congress on Engineering 2018, Volume1,July 4-6, 2018, London, U.K.

[4] K. T. M. Han and B. Uyyanonvara, "A Survey of Blob Detection Algorithms for Biomedical Images," 7th International Conference of Information and Communication Technology for Embedded Systems (IC-ICTES), Bangkok, 2016, pp. 57-60, doi: 10.1109/ICTEmSys.2016.7467122.

Bibliography

[1] Akira Miyata and Shigeo Yaguchi. Equilibrium water content and glistenings in acrylic intraocular lenses. *Journal of Cataract Refractive Surgery*, 30(8):1768 – 1772, 2004. ISSN 0886-3350. doi: https://doi.org/10.1016/j.jcrs.2003.12.038. URL http://www.sciencedirect.com/science/article/pii/S0886335004000641.

[2] Daniele Tognetto, Lisa Toto, Giorgia Sanguinetti, and Giuseppe Ravalico. Glistenings in foldable intraocular lenses1 1none of the authors has a financial or proprietary interest in any material or method mentioned. *Journal of Cataract Refractive Surgery*, 28(7):1211 – 1216, 2002. ISSN 0886-3350. doi: https://doi.org/10.1016/S0886-3350(02)01353-6. URL http://www.sciencedirect.com/science/article/pii/S0886335002013536.

[3] Liliana Werner. Glistenings and surface light scattering in intraocular lenses. *Journal of Cataract Refractive Surgery*, 36(8):1398 – 1420, 2010. ISSN 0886-3350. doi: https://doi.org/10.1016/j.jcrs.2010.06.003. URL http://www.sciencedirect.com/science/article/pii/S0886335010008308.

[4] Akira Miyata, Nobutaka Uchida, Kiyoshi Nakajima, and Shigeo Yaguchi. Clinical and experimental observation of glistening in acrylic intraocular lenses. *Japanese Journal of Ophthalmology*, 45(6):564 – 569, 2001. ISSN 0021-5155. doi: https://doi.org/10.1016/S0021-5155(01)00429-4. URL http://www.sciencedirect.com/science/article/pii/S0021515501004294.

[5] George Beiko and Andrzej Grzybowski. Glistenings in hydrophobic acrylic intraocular lenses do affect visual function. *Clinical ophthalmology (Auckland, N.Z.)*, 7: 2271–2274, 11 2013. doi: 10.2147/OPTH.S52489.

[6] Dogru Murat, Tetsumoto Kazuaki, Tagami Yusaku, Kato Koichi, and Nakamae Katsuhiko. Optical and atomic force microscopy of an explanted acrysof intraocular lens with glistenings. *Journal of Cataract and Refractive Surgery*, 26(4):571–575, 2000.

[7] DeHoog Edward and Doraiswamy Anand. Evaluation of the impact of light scatter from glistenings in pseudophakic eyes. *Journal of Cataract and Refractive Surgery*, 40(1):95–103, 2014.

[8] Bradley S. Henriksen, Krista Kinard, and Randall J. Olson. Effect of intraocular lens glistening size on visual quality. *Journal Cataract Refract Surg*, 41(6):1190–1198, 2015.

[9] Yoriko Takahashi, Takushi Kawamorita, Norihiro Mita, Natsuko Hatsusaka, Shinsuke Shibata, Naoko Shibata, Eri Kubo, and Hiroshi Sasaki. Optical simulation for

subsurface nanoglistening. *Journal of Cataract Refractive Surgery*, 41(1):193—-198, 2015.

[10] Dhaliwal D. K., Mamalis N., Olson R. J., Crandall A. S., Zimmerman P., and Alldredge O. Visual significance of glistenings seen in the acrysof intraocular lens. *Journal of Cataract Refractive Surgery*, 22(4):452–457, 1996.

[11] Wilkins E. and Olson R. J. Glistenings with long-term follow-up of the surgidev b20/20 polymethylmethacrylate intraocular lens. *American journal of ophthalmology*, 132(5):783–785, 2001.

[12] Grzegorz Łabuz, Nic Reus, and Thomas Berg. Straylight from glistenings in intraocular lenses: In vitro study. *Journal of Cataract Refractive Surgery*, 43:102–108, 01 2017. doi: 10.1016/j.jcrs.2016.10.027.

[13] Jan N. Weindler, Grzegorz Łabuz, Timur M. Yildirim, Tamer Tandogan, Ramin Khoramnia, and Gerd U. Auffarth. The impact of glistenings on the optical quality of a hydrophobic acrylic intraocular lens. *Journal of Cataract Refractive Surgery*, 45(7):1020 – 1025, 2019.

[14] Eva Mönestam and Anders Behndig. Impact on visual function from light scattering and glistenings in intraocular lenses, a long-term study. *Acta Ophthalmologica*, 89 (8):724–728, 2011.

[15] Grzegorz Łabuz, Dominik Knebel, Gerd U. Auffarth, Hui Fang, Thomas JTP. van den Berg, Timur M. Yildirim, Hyeck-Soo Son, and Ramin Khoramnia. Glistening formation and light scattering in six hydrophobic-acrylic intraocular lenses. *American Journal of Ophthalmology*, 196:112 – 120, 2018.

[16] Mooren Marrie, Franssen Luuk, and Piers Patricia. Effects of glistenings in intraocular lenses. *Biomedical optics express*, 4:1294–1304, 08 2013.

[17] P. C. Waterman. Matrix formulation of electromagnetic scattering. *Proceedings of the IEEE*, 53(8):805–812, Aug 1965.

[18] Evangelia Filippaki. Glistenings in intraocular lenses and their effect on forward light scatter; an in vitro study. 2015. URL `http://openaccess.city.ac.uk/id/eprint/13594/`.

[19] Heike Biwer, Eva Schuber, Marcus Honig, Bianca Spratte, Martin Baumeister, and Thomas Kohnen. Objective classification of glistenings in implanted intraocular lenses using scheimpflug tomography. *Journal of Cataract Refractive Surgery*, 41(12):2644 – 2651, 2015. ISSN 0886-3350. doi: https://doi.org/10.1016/j.jcrs.2015.06.028. URL `http://www.sciencedirect.com/science/article/pii/S0886335015011219`.

[20] Grzegorz Łabuz, Fernando Vargas-Martín, Thomas J.T.P. van den Berg, and Norberto López-Gil. Method for in vitro assessment of straylight from intraocular lenses. *Biomed. Opt. Express*, 6(11):4457–4464, Nov 2015. doi: 10.1364/BOE.6.004457. URL `http://www.osapublishing.org/boe/abstract.cfm?URI=boe-6-11-4457`.

[21] Liliana Werner, John C. Stover, Jim Schwiegerling, and Kamal K. Das. Light scattering, straylight, and optical quality in hydrophobic acrylic intraocular lenses with subsurface nanoglistenings. *Journal of Cataract Refractive Surgery*, 42(1):148 – 156, 2016. ISSN 0886-3350. doi: https://doi.org/10.1016/j.jcrs.2015.07.043. URL http://www.sciencedirect.com/science/article/pii/S0886335015012055.

[22] Galilei - Dual Scheimpflug Analyzer, . URL https://www.deviceoptical.com/pd-galilei---dual-scheimpflug-analizer.cfm.

[23] Atec. Perkinelmer lambda 35 uv/vis spectrophotometer. URL https://www.atecorp.com/products/perkinelmer/lambda-35.

[24] Oculus optikgeräte gmbh. URL https://www.oculus.de/en/products/visual-test-equipment/c-quant/highlights.

[25] Joseph Colin and Isabelle Orignac. Glistenings on intraocular lenses in healthy eyes: Effects and associations. *Journal of Refractive Surgery*, 27(12):869–875, July 2011. doi: 10.3928/1081597x-20110725-01. URL https://doi.org/10.3928/1081597x-20110725-01.

[26] Bradley S. Henriksen, Krista Kinard, and Randall J. Olson. Effect of intraocular lens glistening size on visual quality. *Journal of Cataract & Refractive Surgery*, 41 (6):1190–1198, June 2015. doi: 10.1016/j.jcrs.2014.09.051. URL https://doi.org/10.1016/j.jcrs.2014.09.051.

[27] Marrie van der Mooren, Roger Steinert, Farrell Tyson, Michelle J.M. Langeslag, and Patricia A. Piers. Explanted multifocal intraocular lenses. *Journal of Cataract & Refractive Surgery*, 41(4):873–877, April 2015. doi: 10.1016/j.jcrs.2015.02.005. URL https://doi.org/10.1016/j.jcrs.2015.02.005.

[28] Grzegorz Łabuz, Nic Reus, and Thomas Berg. Light scattering levels from intraocular lenses extracted from donor eyes. *Journal of Cataract Refractive Surgery*, 43:1207–1212, 09 2017. doi: 10.1016/j.jcrs.2017.06.044.

[29] Difference Between Rods and Cones (with Comparison Chart and Similarities), February 2019. URL https://biodifferences.com/difference-between-rods-and-cones.html.

[30] Edward S. Perkins and Hugh Davson. Human eye, June 22, 2018. URL https://www.britannica.com/science/human-eye.

[31] Dipesh Bhattarai. Application of bessel beams in the human eye, 2019. URL https://trove.nla.gov.au/work/236393797.

[32] Bob Morreale. Anatomy of the eye. URL https://www.brightfocus.org/macular-glaucoma/infographic/anatomy-eye.

[33] B.R. Wooten and George Geri. Psychophysical determination of intraocular light scatter as a function of wavelength. *Vision research*, 27:1291–8, 02 1987. doi: 10.1016/0042-6989(87)90206-9.

[34] Lodovico. Light Scattering, July 2019. URL http://physicsopenlab.org/2019/07/10/light-scattering/.

[35] ELLIOTT DAVID B. Evaluating visual function in catarac. *Optometry and Vision Science*, 11:896–902, 11 1993. doi: 10.1097/00006324-199311000-00006.

[36] Wikipedia. Visual acuity — Wikipedia, the free encyclopedia. http://en.wikipedia.org/w/index.php?title=Visual%20acuity&oldid=940252146, 2020. [Online; accessed 25-February-2020].

[37] Eye Tests, the Eye Chart and 20/20 Vision Explained, . URL https://www.allaboutvision.com/eye-test/.

[38] Contrast Sensitivity Testing, . URL https://www.allaboutvision.com/eye-exam/contrast-sensitivity.htm.

[39] Kooijman A.C. Blanksma L.J Van Den Brom, H.J.B. Clinical and physical measurements of the cataractous lens. *Documenta Ophthalmologica*, 75:247–258, 10 1990. doi: https://doi.org/10.1007/BF00164838.

[40] K Pesudovs and D B Elliott. Refractive error changes in cortical, nuclear, and posterior subcapsular cataracts. *British Journal of Ophthalmology*, 87(8):964–967, 2003. ISSN 0007-1161. doi: 10.1136/bjo.87.8.964. URL https://bjo.bmj.com/content/87/8/964.

[41] Cisneros-Lanuza A., Hurtado-Sarrió M., Duch-Samper A., Gallego-Pinazo R., and Menezo-Rozalén J. L. Glistenings in the artiflex phakic intraocular lens. *Journal of Cataract Refractive Surgery*, 33(8):1405–1408, 2007.

[42] Omni lens. URL http://www.omnilens.in/.

[43] Gennext, Innova, . URL http://www.omnilens.in/portfolio/aspheric-range-gennext-innova/.

[44] Brett Thomes and Tom Callaghan. Evaluation of in vitro glistening formation in hydrophobic acrylic intraocular lenses. *Clinical ophthalmology (Auckland, N.Z.)*, 7: 1529–34, 07 2013. doi: 10.2147/OPTH.S44208.

[45] ImageJ, . URL https://imagej.nih.gov/ij/index.html.

[46] Stanley R. Sternberg. Biomedical image processing. *IEEE Computer*, 16(1):22–34, 1983. doi: 10.1109/MC.1983.1654163. URL https://doi.org/10.1109/MC.1983.1654163.

[47] D. Shvedchenko and Elena Suvorova. New method of automated statistical analysis of polymer-stabilized metal nanoparticles in electron microscopy images. *Crystallography Reports*, 62:802–808, 09 2017. doi: 10.1134/S1063774517050200.

[48] George Stockman and Linda G. Shapiro. *Computer Vision*. Prentice Hall PTR, USA, 1st edition, 2001. ISBN 0130307963.

[49] Wikipedia. Image segmentation — Wikipedia, the free encyclopedia. http://en.wikipedia.org/w/index.php?title=Image%20segmentation&oldid=941491531, 2020. [Online; accessed 25-February-2020].

[50] Prasanna Sahoo, Sasan Soltani, and Andrew Wong. A survey of thresholding techniques. *Computer Vision, Graphics, and Image Processing*, 41:233–260, 02 1988. doi: 10.1016/0734-189X(88)90022-9.

[51] T.W. Ridler and S. Calvard. Picture thresholding using an iterative selection method. *IEEE Transactions on Systems, Man, and Cybernetics*, 8(8):630–632, Aug 1978. ISSN 2168-2909. doi: 10.1109/TSMC.1978.4310039.

[52] Laurent Najman and Michel Schmitt. Watershed of a continuous function. *Signal Processing*, 38(1):99 – 112, 1994. ISSN 0165-1684. doi: https://doi.org/10.1016/0165-1684(94)90059-0. URL http://www.sciencedirect.com/science/article/pii/0165168494900590. Mathematical Morphology and its Applications to Signal Processing.

[53] Serge Beucher and Christian Lantuéjoul. Use of watersheds in contour detection. workshop published, September 1979. URL http://cmm.ensmp.fr/~beucher/publi/watershed.pdf.

[54] Image Segmentation Quality Scores. URL https://www.mathworks.com/matlabcentral/fileexchange/71221-image-segmentation-quality-scores.

[55] Dang Thanh, Surya Prasath, Hieu Le Minh, and Nguyen Hien. Melanoma skin cancer detection method based on adaptive principal curvature, colour normalisation and feature extraction with the abcd rule. *Journal of Digital Imaging*, 33:574–585, 05 2020. doi: 10.1007/s10278-019-00316-x.

[56] Dang Thanh, U***u***gur Erkan, Surya Prasath, Vivek Kumar, and Nguyen Hien. A skin lesion segmentation method for dermoscopic images based on adaptive thresholding with normalization of color models. 04 2019. doi: 10.1109/ICEEE2019.2019.00030.

[57] Dang Thanh, S. Dvoenko, Surya Prasath, and Nguyen Hai. Blood vessels segmentation method for retinal fundus images based on adaptive principal curvature and image derivative operators. 05 2019.

[58] Amos Egel, Lorenzo Pattelli, Giacomo Mazzamuto, Diederik S. Wiersma, and Uli Lemmer. Celes: Cuda-accelerated simulation of electromagnetic scattering by large ensembles of spheres. *Journal of Quantitative Spectroscopy and Radiative Transfer*, 199:103–110, 2017.

[59] Rosalba Saija, Maria Antonia Iati, Ferdinando Borghese, Paolo Denti, Santi Aiello, and Cesare Cecchi-Pestellini. Beyond mie theory: The transition matrix approach in interstellar dust modeling. *The Astrophysical Journal*, 559(2):993–1004, oct 2001.

[60] G. Gouesbet. T-matrix formulation and generalized lorenz–mie theories in spherical coordinates. *Optics Communications*, 283(4):517 – 521, 2010.

[61] Arturo Quirantes, Francisco Arroyo, and Jesús Quirantes-Ros. Multiple light scattering by spherical particle systems and its dependence on concentration: A t-matrix study. *Journal of colloid and interface science*, 240:78–82, 09 2001.

[62] L. L. Holladay. Action of a light-source in the field of view in lowering visibility. *J. Opt. Soc. Am.*, 14(1):1–15, Jan 1927. doi: 10.1364/JOSA.14.000001. URL `http://www.osapublishing.org/abstract.cfm?URI=josa-14-1-1`.

[63] Understanding Luminous flux (lumen) and Illuminance (lux). URL `https://store.yujiintl.com/blogs/high-cri-led/understanding-luminous-flux-lumen-and-illuminance-lux`.

[64] *Appendix 7: Spectral Luminous Efficiency Functions*, pages 678–679. John Wiley Sons, Ltd, 2005. ISBN 9780470024270. doi: 10.1002/0470024275.app7. URL `https://onlinelibrary.wiley.com/doi/abs/10.1002/0470024275.app7`.

[65] Fredrick Seeber. *Fundamentals of photonics*, volume TT79. SPIE, 2010.

[66] Konrad Domke, Krzysztof Wandachowicz, Malgorzata Zalesinska, S. Mroczkowska, and Przemysław Skrzypczak. Large-sized digital billboards hazard. *International Journal of Design Nature and Ecodynamics*, 7:367–380, 12 2012. doi: 10.2495/DNE-V7-N4-367-380.

Appendix A

Minor Research : Simulation of Multiple Light Scattering in Intraocular lens with glistenings by T-Matrix

A.1 Introduction

Glistenings are micro vacuoles which appear small bubbles in IOL after the cataract surgery. Natural aging of the eyes is the main cause of cataract is human eyes in which protein in the lens clump together forming clusters and decrease the vision quality. Cataract surgery is required when the vision of the patients is not clear so that the common treatment to cataract is surgical removal of natural lens and implant intraocular lens. Since IOL is aqueous environment, temperature changes between human body and manufacturing process can void the water into gaps and it is called glistening. Due to glistening problem in an IOL, retinal image quality can be affected by scattering of light. Typically, the acuity and the density of light receptors depends on the focus of visual stimulus on the fovea within the neurosensory retina. Glistenings can cause scattering and result in unclear vision. In addition, light scattering may produce halos or glare due to the increasing of diffused light on the retina. In ophthalmology, the effect of glistening on quality of visual perception can be assessed in clinical test by using best-corrected visual acuity,contrast sensitivity, glare testing or wavefront measurements in human eyes. In contrast to these clinical approaches, this research investigates the light scattering problem in simulation from electromagnetic point of view.

A.1.1 Purpose of study

The purpose of this study is to calculate and simulate the light scatter contribution induced by microvacuoles by using T-Matrix (transition matrix) theory. In this research, the proposed method calculated the total electric field by multiple microvacuoles after scattering in IOL due to glistenings and visualize how glistening particles are in IOL depending upon the different grade of glistenings.To emphasize our research contribution, this research is the first usage of T-matrix method for modeling the light scattering through multiple glistening in IOL material.

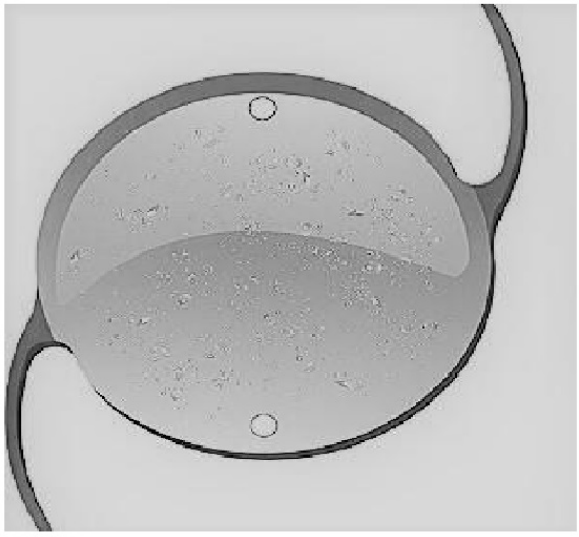

Figure A.1: Glistening formation inside intraocular lens

A.1.2 Scope of study

The scope of this research is lied on small reflections of light by micro vacuoles cause forward light scattering in IOL. There are several research from clinical studies investigate the correlation between glistenings and forward light scatter problems. However, methods to measure the intraocular lens can be categorized into optical methods and psychophysical methods. The former method is a direct measurement of forward light scattering by using specific camera or sensors such as straylight meter (C Quant log) and Scheimpflug photography[67][68] [69] and the latter analyzed from mathematically modeling, and was verified by calculations with Mie scattering theory [70][71].

In optical method, intraocular light scatter problems are reported from the clinical point of view in which the assessment is reviewed according to the records of patients who had cataract surgeries. In Monestam el al.,2011 [68], patients in this study group are approximately after 1 year of cataract surgery and examined the light scattering by using Scheimpflug photography. This study is required to participate by the patients and calculated light scattering manually and furthermore, it is time consuming and costly to research. In psychophysical method, some researches are also proved from the point of view of Physics by using light scatter equations to identify the amount of intensity decreasing on account of glistenings and therefore, the approximated number of results can be differed with the real problem. Nevertheless, quality of visual functions can be reduced due to glistenings and verified from different point of views.

This research is conducted from information science point of view combining with optics physics to simulate how electric fields are scattered according to the properties of glistenings. Therefore, glistening characteristics are important parameters to calculate the total electric field. Many research reports that glistening can be different size, num-

bers, shapes and refractive index which can affect on light scattering. However, shape of glistenings are assumed to be sphere in this research. To overcome the limitation, T-matrix method can be further expanded arbitrary shapes, it can be extended by our future works. Our current works focus on simulation multiple light scattering problem in IOL by using T-matrix method with spherical glistening.

A.2 Literature review

In recent years, there are several studies related to glistening characteristics and method to assess glistenings in IOL. Glistenings can be found with different characteristics such as size, number and reflective indices which depend on the material of the lens. In fact, glistenings are small water inclusions in IOL which is shown in figure A.1 and thus, the different size of glistenings can be found. According to previous studies, glistenings has been reported with the diameter range from 10 to 20 µm by Dogru et al. (2000) [72]. However, the different size of glistenings have been found by DeHoog et al. (2014) and experimented with 2 to 200 µm in diameter [70] but Henriksen et al (2015) presented as two groups: 6 to 25 µm or greater than 25 µm [67]. Recently, the size of glistening is significantly varied and observed by Takahashi et al. (2015) that the size range is between 1 µm and 120 µm [73] but the optical simulation in that research was implemented by three different sizes: 100 nm, 150 nm, and 200 nm.

A.2.1 Grade of glistenings

The number of glistening in IOL is also important factor for grading of glistening. In fact, glistenings are graded in intraocular lens by clinicians through slit lamp. They manually counted the number of glistenings and report as different grades. Therefore, several studies described about grading by number of glistenings present in IOL. Firstly, three grades of glistenings such as 1 +,2 + and 3 + has been reported by Dhaliwal et al. (1996) [74]. Moreover, glistening grades are recorded as 0 to 3+ by Wilkins and Olson (2001) in which 0 for no glistenings, 1+ for less than 10, 2+ for 10 to 50 and 3+ for more than 50 [75] .Yet, Cisneros-Lanuza et al. (2007) proposed glistening appearance in IOL and graded 1+ for 10 to 20, 2+ for 20 to 30, 3+ for 30 to 40 and 4+ for more than 40 glistenigs [76]. However, glistening number are classified and measured per mm2 by Geniusz et al. (2015) where grade 0 (none), grade 1 (1-100), grade 2 (101-200), grade 3 (201-500) and grade 4 (more than 500) [77]. According to previous studies, grading scales can be represented by occurrence of glistening numbers in IOL, but common agreement is not found on defining glistening's grading.

A.2.2 Problem statements

The main problem of glistenings has been studied and light scattering is the impact of glistenings contribution in IOL [70] [67] [68] [69].When the incident light pass through

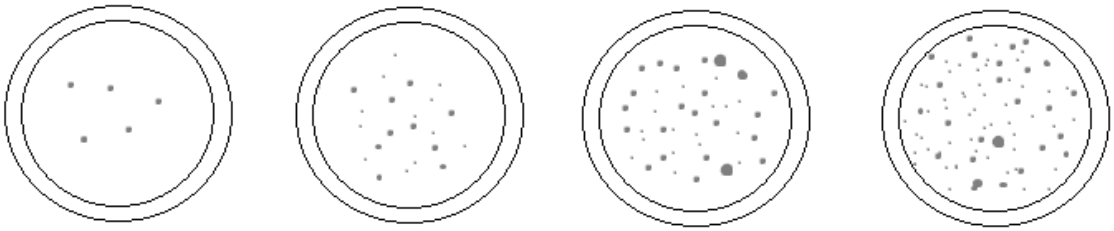

Figure A.2: Different grades of glistenings in IOL depending upon the number of formations

a medium called intraocular lens, light can be transmitted, reflected and scattered to random directions due to glistenings and moreover, it can be absorbed in the medium. Light scattering due to small water inclusions called microvacuoles propagates in directions other than backward and forward, leading to an increase in intraocular straylight and a decrease in light transmittance to the retina.

The previous research [67] [68] [69] proposed light scattering problem in IOL from laboratory investigation and evaluated by using medical equipment such as straylight meter (C Quant log) and Scheimpflug photography. Nevertheless, other research analyzed from mathematically modeling, and was verified by calculations with Mie scattering theory [70][71]. If particle shapes are sphere, Mie theory is more appropriate for light scattering problem. Since different grades of glistenings have been found in IOL, multiple light scattering occurs and single light scattering problem by a sphere is not sufficient to satisfy the problem.

Several studies report the light scattering from one sphere and multiple scattering for IOL has not considered.For the real IOL problem, light transmittance to the retina which can interfere by glistenings is not only for single particle problem, but also multi-glistenings is also considerable for visual quality. If the glistening particles are far from one another then each particle scatters light as if the other particle was not there, and the total light-scattering is simply twice the scattering of an individual particle. However, if the particles are brought closer together, so that their surfaces are from one another, then their scattering volumes begin to overlap. Therefore, the total scattering volume from the two glistenings is less than the sum of the two-individual scattering volumes. When light that enters the overlap volume, light can scatter less efficiently than light that enters a part of the nonoverlapping scattering. Therefore, light scattering for group glistening is another problem statement for our research and we follow the above process as single glistening scattering in IOL.

In this research, T-Matrix method is applied for light scattering in IOL by mathematical modelling and optical simulation. Additionally, T-matrix method calculated a pair of

spherical particles as a single scatterer and has originally been developed by Waterman [78] .The proposed methodology aims to simulate multiple scattering in IOL although many researches have been processed only for light scattering of single glistening in IOL by using Mie Scattering Theory. As a result, light scattering of electric field through glistenings in IOL can be calculated and simulated.

A.3 Methodology

The impact of glistening in IOL cause light scattering which depends on the refractive index between the vacuoles and the lens material, as well as the size, density and shape of the glistenings. In this paper, the scattering problem are discussed into two sections: Scattering Parameter and T-Matrix method for calculation of light scattering. In fact, the data to calculate light scattering has obtained from the previous literatures [72][70][67][73][74][75][76][77] and described in the next section as Scattering Parameter. Moreover, the scattering of light by glistening clusters is calculated by using the multiple-sphere T-Matrix method and simulated with CELES, Matlab toolbox which runs on graphics processing units (GPUs).

A.3.1 Scattering Parameter

During optical simulation, glistening sizes are set as 80nm, 100nm and 120nm because of the run time environment (GPU) is not acceptable for very large spheres and it takes time to run. The microvacuoles were distributed randomly in spherical coordinate system of IOL. The refractive indices of glistenings and IOL were assigned to 1.336 and 1.5. Firstly, initial excitation for the simulations is used a Gaussian beam with a beam waist of 4 µm. The wavelength parameter(λ) is given 550nm because human eyes' visibility wavelength is in the range between 390nm and 720nm. Since there is no standard defining the glistening's grading, the number of glistening in each simulation is grouped as grade 1 (less than 10), grade 2 (10-50), grade 3 (50-100) and grade 4 (100-500).

A.3.2 T-Matrix

Light is an electromagnetic wave which is discovered by Maxwell. Therefore, light scattering in this research is assumed as electromagnetic scattering which can be explained by electric field(E) and magnetic field(H). In addition, light scattering in IOL was calculated by using T-Matrix method which is based on expansion of incident, and the scattered field into a series of spherical vector wave functions [79]. Total electric field(E) is written as a sum of incident and scattered fields for ith particle.

$$\overrightarrow{E} = \overrightarrow{E^I} + \overrightarrow{E^s} \tag{A.1}$$

In fact, T-matrix is a particle response matrix which transforms the incident field expansion coefficients to the scattered field coefficients. Moreover, particle shape, size, refractive index and the orientation of the particle are correlated to T-matrix. Therefore, the scattered field can be calculated for any incident field and any direction when T-matrix is known for a particle. To calculate for one sphere, the total electric field is the sum of an incident field and the scattered field. For multiple particles, the incoming field

for each ith particle is the sum of the initial excitation and the scattered field of all other N spheres:

$$\mathrm{E}_{in}^{i}(r) = \mathrm{E}_{i}(r) + \sum_{i' \neq i}^{N} \mathrm{E}_{s}^{i'}(r) \tag{A.2}$$

Since T-matrix approach is from electromagnetic framework, the interaction between an illumination wave and scattering particles relies on the expansion of the incident wave and of the scattered wave in terms of vector spherical wave functions (SVWFs) [80] in which RgM, RgN means the regular wave functions and M, N refers to the singular wave functions.(Appendix 6.1)

$$\mathrm{E}_{i}(r) = \sum_{n=1}^{\infty} \sum_{m=-n}^{n} [a_{mn} RgM_{mn}(kr) + b_{mn} RgN_{mn}(kr)] \tag{A.3}$$

$$\mathrm{E}_{s}(r) = \sum_{n=1}^{\infty} \sum_{m=-n}^{n} [p_{mn} M_{mn}(kr) + q_{mn} N_{mn}(kr)] \tag{A.4}$$

where k (wave number) $=2\pi/\lambda$, λ is the wavelength, r means the position vector and degree n and order m. According to Maxwell's equations, the scattered field coefficients p_{mn} and q_{mn} can be calculated from the incident field coefficients a_{mn} and b_{mn} by using a transition matrix.

$$\mathrm{p}_{mn} = \sum_{n'=1}^{\infty} \sum_{m'=-n'}^{n'} [T^{11}_{mm'nn'} a_{m'n'} + T^{12}_{mm'nn'} b_{m'n'}] \tag{A.5}$$

$$\mathrm{q}_{mn} = \sum_{n'=1}^{\infty} \sum_{m'=-n'}^{n'} [T^{21}_{mm'nn'} a_{m'n'} + T^{22}_{mm'nn'} b_{m'n'}] \tag{A.6}$$

Equation (6) can be written in a compact form as:

$$\begin{bmatrix} p \\ q \end{bmatrix} = T \begin{bmatrix} a \\ b \end{bmatrix} = \begin{bmatrix} \mathrm{T}_{11} & \mathrm{T}_{12} \\ \mathrm{T}_{21} & \mathrm{T}_{22} \end{bmatrix} \begin{bmatrix} a \\ b \end{bmatrix} \tag{A.7}$$

However, T-matrix takes account of mn indices, and thus a new variable l_{max} is defined as n(n+1) +m to know the maximum level of the matrix. Therefore, equation A.6 can be written in details according to the levels of matrix (l_{max}).

$$\begin{bmatrix} p \\ q \\ \cdots \\ \cdots \\ \mathrm{p}_{lmax} \\ \mathrm{p}_{lmax} \end{bmatrix} = \begin{bmatrix} \mathrm{T}^{11}_{11} & \mathrm{T}^{12}_{11} & \cdots & \cdots & \mathrm{T}^{11}_{1,lmax} & \mathrm{T}^{12}_{1,lmax} \\ \mathrm{T}^{21}_{11} & \mathrm{T}^{22}_{11} & \cdots & \cdots & \mathrm{T}^{21}_{1,lmax} & \mathrm{T}^{22}_{1,lmax} \\ \cdots & \cdots & \cdots & \cdots & \cdots & \cdots \\ \cdots & \cdots & \cdots & \cdots & \cdots & \cdots \\ \mathrm{T}^{11}_{lmax,1} & \mathrm{T}^{12}_{lamx,1} & \cdots & \cdots & \mathrm{T}^{11}_{lmax,lmax} & \mathrm{T}^{12}_{lmax,lmax} \\ \mathrm{T}^{21}_{lmax,1} & \mathrm{T}^{22}_{lmax,1} & \cdots & \cdots & \mathrm{T}^{21}_{lmax,lmax} & \mathrm{T}^{22}_{lmax,lmax} \end{bmatrix} \begin{bmatrix} \mathrm{a}_1 \\ \mathrm{b}_1 \\ \cdots \\ \cdots \\ \mathrm{a}_{lmax} \\ \mathrm{b}_{lmax} \end{bmatrix} \tag{A.8}$$

However, $p = T \cdot a$ is used as a short description for next equations from equation A.7 and A.8 where $p = [p_{mn}, q_{mn}]$ and $a = [a_{mn}, b_{mn}]$. However, the purpose of using T-matrix is that allows a pair of spherical particles can be calculated a single scatterer [81]. Yet,

the multiple scattering takes account of the incoming field coefficients with the initial field and sum of scattering field coefficients from all particles. The sphere centered T^{ji} matrix is converted to the cluster-center T-matrix based on a single origin of the cluster.

$$\mathrm{p}^j = \mathrm{T}^j(\mathrm{a}^i + \sum_{i \neq j} \mathrm{A}^{ji}\mathrm{p}^i) \tag{A.9}$$

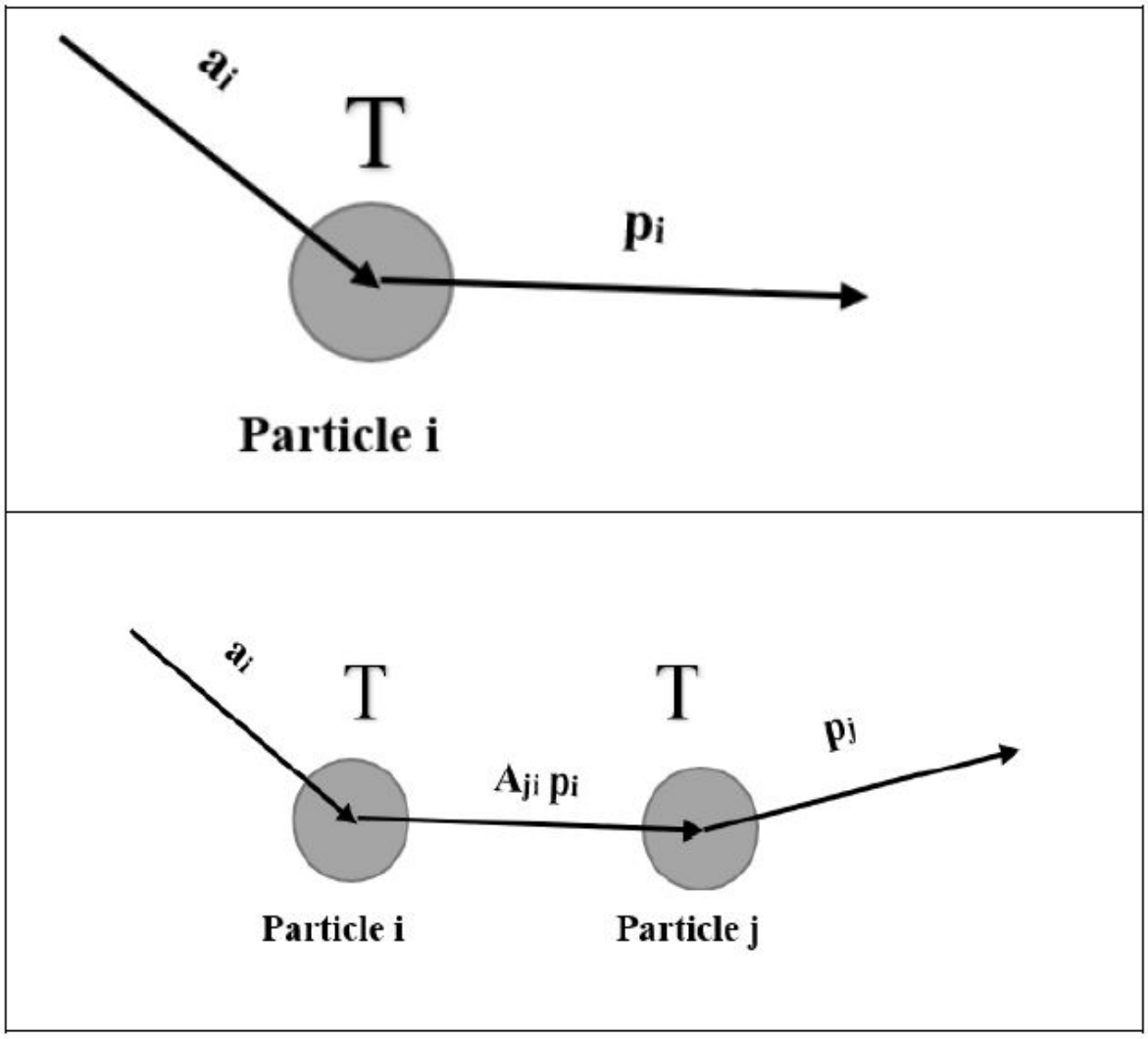

Figure A.3: Block Diagram of Transition matrix in one particle and between two particles in which scattering field coefficients are calculated from incident field coefficients

The above equation is scattered field coefficient for sphere j can be calculated through transition matrix of particle j, incident field coefficient of sphere i and A^{ji} matrices. A^{ji} matrices is the electromagnetic interaction between two particles i and j, moreover it is also related to the distance and orientation between these two particles. Therefore, tran-

sition matrix transforms the expansion coefficient of the incident field into the expansion of individual scattered field.

$$\mathrm{p}^j = \sum_i \mathrm{T}^{ji}\mathrm{p}^i \tag{A.10}$$

Finally, multiple scattering problem is achieved as a single expansion of the particles that can be achieved from the scattered field expansions of the individual spheres where a and p are the incident and scattered field coefficients, B is also the matrices of the electromagnetic interaction between two particles which is similar to A matrix.

$$p = \sum_j \mathrm{p}^j = \sum_{j,i} \mathrm{B}^j\mathrm{T}^{ji}\mathrm{a}^i = \sum_{j,i} \mathrm{B}^j\mathrm{T}^{ji}\mathrm{B}^i a = Ta \tag{A.11}$$

A.4 Simulation

In this research, the input data is the properties of glistenings which are used from academic literature and simulated with CELE program. CELE is used to visaulize how mulitple light scattering problems occurs in IOL because simulation of the scattering process can help to understand the scattering characteristics. To simplify the computational simulation, sphere particles are used while in reality particles usually do not show such simple structures. For our future work, we prefer three-dimensional model describing the particle shape will be used. However, there are many research in which glistenings are assumed to be spheres and different grades of glistenings is proposed. In this simulation, 4 different grades are selected to analyze so that the number of glistenings will be varied.

Moreover, size of glistenings are also specified 3 types in this simulation: 80 nm, 100nm and 120nm.Due to the limitation of memory to run this simulation, the particle size more than 150 is not appropriate from grade 2 glistenings. figure A.4,A.5,A.6, and A.7 show position of spherical glistenings in IOL with coordinate system and how total electric field after incident wave is scattered through the particles since glistening is densely closed and multiple scattering occurred in this condition. In fact, second figure from figure A.4,A.5,A.6, and A.7 is plotting the result from Equation (1) as the function: $E(r) = E_i(r) + E_s(r)$. Although different grades of glistenings are changed in this simulation, three different IOL sizes are randomly selected. Near-field intensity is not affected while glistenings are freely located. For example, the first pictures of figure A.4,A.5,A.6, and A.7 show that the number of glistenings and location of those particles are related to total electric field scattering. However, the densely packed glistening (grade 3 and grade 4) from the second pictures of figure A.4,A.5,A.6, and A.7 show that electric field intensity is stronger because of the coupling effect from multiple light scattering through these particles.

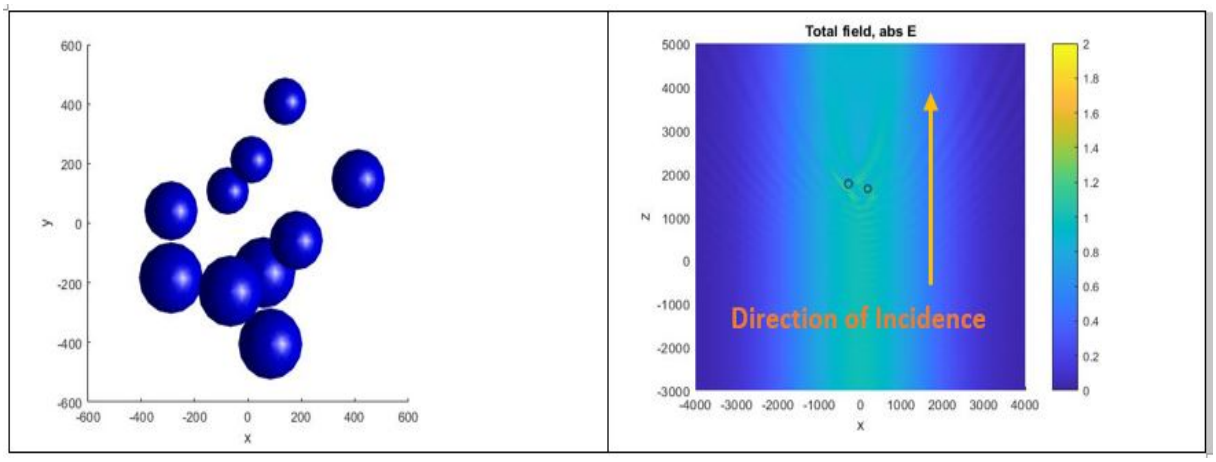

Figure A.4: Position of Grade 1 glistenings and total electric field after light scattering

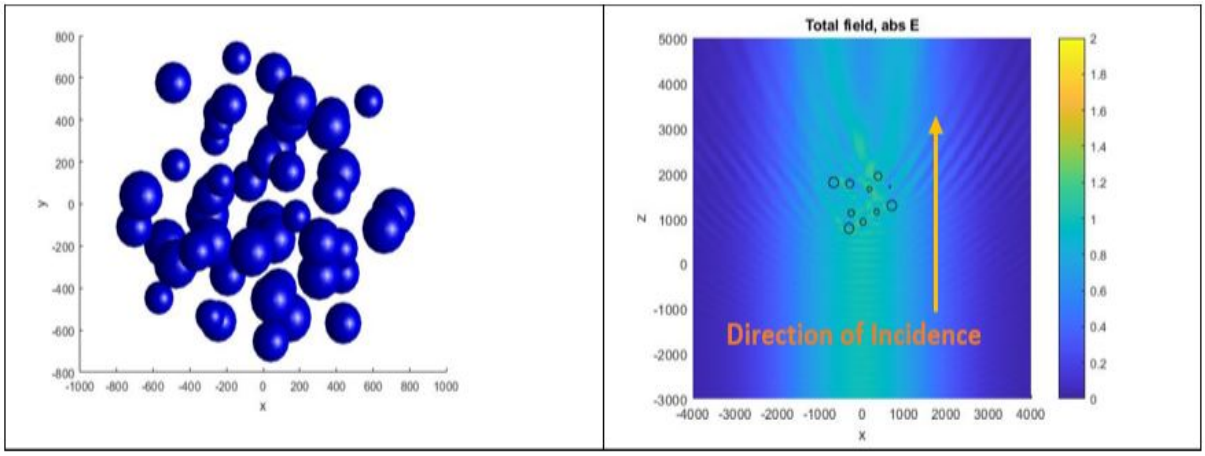

Figure A.5: Position of Grade 2 glistenings and total electric field after light scattering

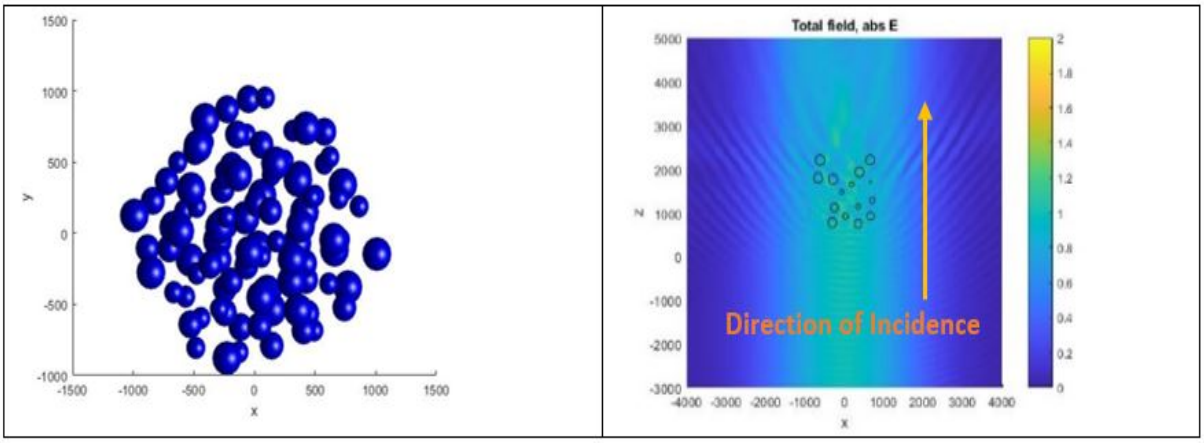

Figure A.6: Position of Grade 3 glistenings and total electric field after light scattering

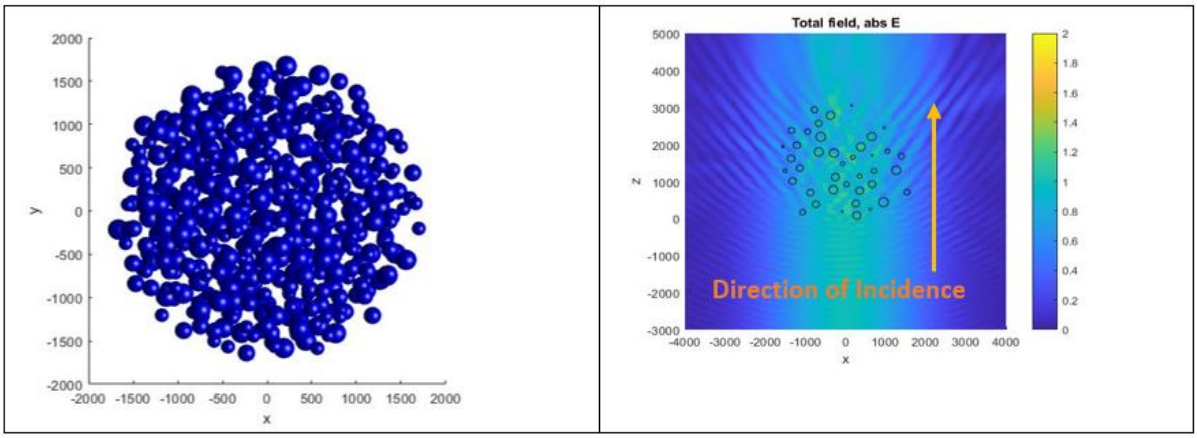

Figure A.7: Position of Grade 4 glistenings and total electric field after light scattering

A.5 Discussion

The experiment result of the previous sections is discussed and concluded here. Multiple light scattering due to glistenings have been discussed. Since glistenings are very small water inclusions, the shape of glistening is challenging for light scattering problem. In this research, we simulated multiple light scattering problem in IOL by using T-matrix method with spherical glistening. As a result, our simulation can visualize how electric field of light is scattered in IOL material from electromagnetic point of view. Although this research has defined shape of glistenings to be sphere, several studies have reported the limitation of Mie's spherical assumption. To overcome the limitation, T-matrix method can be further expanded arbitrary shapes. The possible next step of this research is to apply T-matrix method with real glistening shapes which are reconstructed as 3D model from microscopic images. Therefore, glistening data from 3D model will be more detailed in defining multiple light scattering problems because near field and coupling effect of glistenings can be accurately calculated.

A.6 Appendix

A.6.1 Spherical Vector Wave

$$M_{mn}= z_n(\mathrm{kr})[\mathrm{im}\ \frac{P_n^m(cos\theta)}{sin\theta}\hat{\theta} - \frac{dP_n^m(cos\theta)}{d\theta}\hat{\theta}\ ]\ e^{im\phi}$$

$$N_{mn}= \mathrm{n(n+1)}\ \frac{z_n(kr)}{kr}P_n^m(cos\theta)e^{im\phi}\hat{r} + \frac{1}{kr}\frac{d(rz_n(kr))}{dr}\ [\ \frac{dP_n^m(cos\theta)}{d\theta}\hat{\theta} + \mathrm{im}\ \frac{P_n^m(cos\theta)}{sin\theta}\hat{\phi}\ ]\ e^{im\phi}$$

where $z_n(x)$ can be spherical Bessel functions($j_n(x)$ or $y_n(x)$), Hankel function of the first kind $h_n^1(x)P_mn(x)$ is the associated Legendre function and (r, θ, ϕ)are the unit vectors in spherical coordinates.

A.6.2 Spherical Bessel Function and Hankel Function

The spherical Bessel differential equation is defined as

$z^2 = \frac{d^2}{dz^2}\ Z_n(z) + 2z\ \frac{d}{dz}\ Z_n\ (z) + (\ z^2 - n(n+1))\ Z_n\ (z) = 0$

Where n is a positive integer and z is a complex number. The spherical Bessel function $j_n(z)$ can be defined wtih the power series expansion.

$j_n(z) = 2^n\ z^n \sum_{k=0}^{\infty} \frac{(-1)^k (k+n)!}{k!(2k+2n+1)!}\ z^{2k}$

The spherical Hankel function is defined as:

$h_n^1(z) = j_n(z) + i n_n(z)$

$h_n^2(z) = j_n(z) - i n_n(z)$

where $h_n^1(z)$ and $h_n^2(z)$ first and second order Hankel function respectively.

References

[67] Bradley S. Henriksen, Krista Kinard, and Randall J. Olson. Effect of intraocular lens glistening size on visual quality. *Journal Cataract Refract Surg*, 41(6):1190–1198, 2015.

[68] Eva Mönestam and Anders Behndig. Impact on visual function from light scattering and glistenings in intraocular lenses, a long-term study. *Acta Ophthalmologica*, 89 (8):724–728, 2011.

[69] Grzegorz Łabuz, Dominik Knebel, Gerd U. Auffarth, Hui Fang, Thomas JTP. van den Berg, Timur M. Yildirim, Hyeck-Soo Son, and Ramin Khoramnia. Glistening formation and light scattering in six hydrophobic-acrylic intraocular lenses. *American Journal of Ophthalmology*, 196:112 – 120, 2018.

[70] DeHoog Edward and Doraiswamy Anand. Evaluation of the impact of light scatter from glistenings in pseudophakic eyes. *Journal of Cataract and Refractive Surgery*, 40(1):95–103, 2014.

[71] Mooren Marrie, Franssen Luuk, and Piers Patricia. Effects of glistenings in intraocular lenses. *Biomedical optics express*, 4:1294–1304, 08 2013.

[72] Dogru Murat, Tetsumoto Kazuaki, Tagami Yusaku, Kato Koichi, and Nakamae Katsuhiko. Optical and atomic force microscopy of an explanted acrysof intraocular lens with glistenings. *Journal of Cataract and Refractive Surgery*, 26(4):571–575, 2000.

[73] Yoriko Takahashi, Takushi Kawamorita, Norihiro Mita, Natsuko Hatsusaka, Shinsuke Shibata, Naoko Shibata, Eri Kubo, and Hiroshi Sasaki. Optical simulation for subsurface nanoglistening. *Journal of Cataract Refractive Surgery*, 41(1):193—-198, 2015.

[74] Dhaliwal D. K., Mamalis N., Olson R. J., Crandall A. S., Zimmerman P., and Alldredge O. Visual significance of glistenings seen in the acrysof intraocular lens. *Journal of Cataract Refractive Surgery*, 22(4):452–457, 1996.

[75] Wilkins E. and Olson R. J. Glistenings with long-term follow-up of the surgidev b20/20 polymethylmethacrylate intraocular lens. *American journal of ophthalmology*, 132(5):783–785, 2001.

[76] Cisneros-Lanuza A., Hurtado-Sarrió M., Duch-Samper A., Gallego-Pinazo R., and Menezo-Rozalén J. L. Glistenings in the artiflex phakic intraocular lens. *Journal of Cataract Refractive Surgery*, 33(8):1405–1408, 2007.

[77] Jan N. Weindler, Grzegorz Łabuz, Timur M. Yildirim, Tamer Tandogan, Ramin Khoramnia, and Gerd U. Auffarth. The impact of glistenings on the optical quality of a hydrophobic acrylic intraocular lens. *Journal of Cataract Refractive Surgery*, 45(7):1020 – 1025, 2019.

[78] P. C. Waterman. Matrix formulation of electromagnetic scattering. *Proceedings of the IEEE*, 53(8):805–812, Aug 1965.

[79] Rosalba Saija, Maria Antonia Iati, Ferdinando Borghese, Paolo Denti, Santi Aiello, and Cesare Cecchi-Pestellini. Beyond mie theory: The transition matrix approach in interstellar dust modeling. *The Astrophysical Journal*, 559(2):993–1004, oct 2001.

[80] G. Gouesbet. T-matrix formulation and generalized lorenz–mie theories in spherical coordinates. *Optics Communications*, 283(4):517 – 521, 2010.

[81] Arturo Quirantes, Francisco Arroyo, and Jesús Quirantes-Ros. Multiple light scattering by spherical particle systems and its dependence on concentration: A t-matrix study. *Journal of colloid and interface science*, 240:78–82, 09 2001.